Rational manipulation of substrate-supported graphene by heterogeneity of substrate surface and material composition

by

Talal Al-Mulla

S.B., Massachusetts Institute of Technology (2013)

Submitted to the Department of Civil and Environmental Engineering
in partial fulfillment of the requirements for the degree of

Master of Science in Civil and Environmental Engineering

at the

MASSACHUSETTS INSTITUTE OF TECHNOLOGY

February 2017

Signature redacted

Author .....
Department of Civil and Environmental Engineering
October 31, 2016

Signature redacted

Certified by .....
Markus J. Buehler
Professor of Civil and Environmental Engineering
Thesis Supervisor

Signature redacted

Accepted by .....
Jesse Kroll
Professor of Civil and Environmental Engineering
Chair, Graduate Program Committee

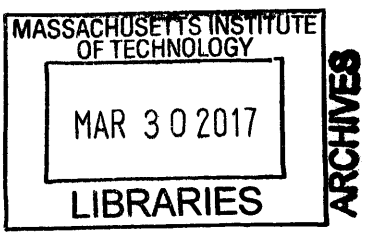

Rational manipulation of substrate-supported graphene by heterogeneity of substrate surface and material composition

by

Talal Al-Mulla

Submitted to the Department of Civil and Environmental Engineering
on October 31, 2016, in partial fulfillment of the
requirements for the degree of
Master of Science in Civil and Environmental Engineering

Abstract

In many graphene-based devices graphene is adhered to a substrate that influences its performance, rather than being present in a free standing form. The interaction of graphene with these substrates can lead to deformations that give rise to out-of-plane architectures with new properties such as superhydrophobicity, opened electronic band gap, and higher in-plane rigidity. Earlier experiments and simulations with graphene-substrate interfaces demonstrating reversible and repeatable stacking of out-of-plane buckled graphene to create ridges, which are stacked protrusions of graphene, warrant a detailed understanding of the underlying mechanisms of graphene ridge formation, especially for design of tailored nanostructures. Ridges are created through substrate-mediated compression of graphene, therefore, these ridges should be related to the graphene-substrate interface. It is unknown what the direct effect of the substrate on ridge formation is besides the work done studying graphene's mechanical response to compression. It is necessary to understand how the substrate affects graphene deformation in order to fully utilize the range of accessible graphene deformation shapes.

To systematically study the formation of ridges in graphene, molecular dynamics simulations are performed to characterize the deformation of graphene on substrate during and after axial compression of graphene nanoribbons, high aspect ratio (10:1) single layer sheets of graphene in this work. This is done to investigate the hypothesis that graphene deformation depends on the underlying substrate in terms of corrugation wavelength and amplitude and graphene-substrate adhesion energy. In the first part of this thesis a quantitative scheme is formulated to characterize and predict these deformations. A critical value of interfacial adhesion energy marks a transition point that separates two deformation regimes of graphene on substrate under uniaxial compression; the deformation regimes are binary featuring the stacking of graphene after buckling in one case and no stacking, otherwise.

These ridges are a product of the graphene limit point buckling, where growing out-of-plane folds of graphene stack and self-adhere. In the second part of this thesis, after establishing the role of substrate and key interfacial properties, the atomistic

mechanisms underlying the formation, evolution, and localization of graphene ridges are investigated using fracture mechanics theory and molecular dynamics simulations. It is shown that there is no intrinsic characteristic length scale over which to achieve certain graphene shapes or see any repeated shapes as suggested in previous experiments, but instead these shapes can be tuned by substrate selection and design, a novel approach presented in this thesis. Moreover, a major result of this work is that the location and density of surface features in graphene-substrate systems can be controlled by substrate engineering at nanoscale resolutions, which could be used for developing graphene-based devices with a more efficient use of material, or with tailored distribution of surface futures that lead to specific applications. Efficiency gains can be made through use of less material and more controlled spacing of graphene ridges. The immediate impact of this work is most clearly realized in large scale manipulation of graphene where targeted deformations of different regions of the same graphene sheet can be executed using a single rationally designed substrate. Shifting the mindset from using the substrate as a stage, but as a tool, opens up the potential for more intricate graphene deformations at the nanoscale.

Thesis Supervisor: Markus J. Buehler
Title: Professor of Civil and Environmental Engineering

To my family and the one and only love of my life.

Acknowledgments

It always seems like any worthy undertaking is toilsome and difficult. In truth these overbearing feelings are quickly extinguished and their nonexistence realized at the close. All that is left is to reaffirm appreciation to the key persons that made the past journey truly bearable and at times overly delightful. I do not wish to thank here, for the first time, all the brilliant individuals that have carried me along the way. To do so would be an insult and an ingratitude that I have committed because any thanks now is indeed too late. I merely wish to reiterate and put pen to paper the thanks I have owed and hopefully given.

My initial thanks go to my immediate environment in which this thesis was able to stem and grow. I would like to extend my gratitude towards my adviser, Markus J. Buehler, for his support and guidance. I would also like to thank everyone in the Laboratory for Atomistic and Molecular Mechanics for creating a wonderful, supportive working environment including Dieter Bresnan Brommer, Shu-Wei Chang, Chia-Ching Chou, Leon Sokratis Scheie Dimas, Tristan Giesa, Kai Jin, Zhao Qin, and Max Solar. Thank you also to GangSeob Jung for teaching me so much about Korea and molecular dynamics and being Ringo. I would also like to thank Chun-Teh Chen, first for being Skye and then Celeste and working with me on that continuum mechanics project, creating simulations on the fly.

Away from lab there have been many mentors and friends that I have gained so much from. I would take this chance to express my utmost respect and thanks to Mostafa Youssef for a perceptive gaze and sensible conversations. Remarkably, my closest friends form a quaint acronym in AYA. Among them first is the voice of reason from so long ago, Afsah Shafquat, who can never go unmentioned in any acknowledgments section. Thank you for being my friend. Yazeed Al-Rashed, nobody has ever taken me for a run through the Boston Financial District. Thank you for all the adventures. I have to also say thank you to Afrah Shafquat, for all the memories. To all the names I have not mentioned you have earned my sincerest apologies, over and above my thanks.

I have also been fortunate enough to meet Koshka and Grace during my time here. Koshka Semc, your indomitable personality and flair for life always cheered me up when I needed cheering up. Grace Xiang Gu, thank you for being the positive ray of hope and optimism in my latter years in the group. Without you I would have given up so many times. I owe you so much. I will never forget and truly appreciate your selflessness. It is rare to make truly strong bonds with others, and I thank you for the opportunity to forge such a bond with you. You are the personification of Life of more Learning. It is hard to find something you love, but you make it easy with your dedication and conviction. Thank you both.

And I would literally and figuratively not have been able to accomplish any of this without my parents' love and support. Studying abroad means seeing less of your family, but absence makes the heart grow fonder, and technology makes the world grow smaller. All the FaceTime calls made so much feel that much easier. And to my brother who has always been there for me when I needed him I say: you are the best brother anyone could ask for. When you started college and we made a home away from home our brotherhood grew stronger. Mom, thank you for making the trips across continents and an ocean to prepare home-cooked food for us when we couldn't be home. No amount of thanks would do justice to convey my appreciation, gratitude, and love to my mom and dad and brother. That will take me the rest of my life.

Cambridge, MA
October 31, 2016

THIS PAGE INTENTIONALLY LEFT BLANK

Contents

List of Figures

4-3 **Atomistic ridge formation mechanism.** Graphene is compressed up to a critical force after which delaminated buckling occurs followed by a transient tearing off of the substrate (A) that leaves behind a large delaminated area. As compression continues the edges of the delaminated area re-adhere (B) and the graphene film starts to grow out of plane (C). In part due to the original large delaminated area at buckling, there is some free-standing graphene held up above the substrate-supported graphene which does not get compressed by the substrate creating a pinching effect (D) at the base of the delaminated region of graphene. Further compression guarantees self-adhesion (E) of the graphene creating a ridge after this pinching in effect and grows the ridge taller (F). Self-adhesion (D $\rightarrow$ E) is energetically favorable because it decreases the area of free surface caused by delamination and less graphene is subject to bending. Load displacement curves show a linear increase in load as the graphene-substrate composite is compressed up to the point of initial delamination. This point corresponds to the attainment of the critical energy release rate at the interface, delamination initiation, dissipation of stored strain energy (A) in the graphene nanoribbon, and the onset of delaminated buckling. 74

List of Tables

THIS PAGE INTENTIONALLY LEFT BLANK

Chapter 1

Introduction

Graphene, a two-dimensional sp^2-hybridzed honeycomb lattice of carbon atoms, has great promise for use in nanoelectronics [4, 5], nano devices [6, 7], and biomedical sensors [8] due to its ultrathin nature and outstanding electrical [9–11], mechanical [12], thermal [13], and optical properties [14–16]. A key property of graphene is its high flexibility complementing its high strength, which allows it to assume various bent configurations in many novel applications [17, 18]. Recent experimental work has shown controlled changing in the topography of planar multilayer graphene to induce super hydrophobicity and to mimic muscle actuation through an applied voltage across a graphene substrate interface [19]. This control of graphene shape and topology opens new avenues for applications of graphene materials, increasing the versatility of graphene as a building block of new electrochemical capacitors [20, 21], photodetection devices [22], biosensors [23], to name a few, and as a platform for novel nano devices.

Despite the extensive attention dedicated to graphene, it still remains an astounding material for research not only for its well-known remarkable mechanical [12], electrical [24], thermal [13], and optical [25, 26] properties, but as of late, also due to its micromechanical response to deformation [27–30]. In fact, graphene being compressed on a substrate generates many different shapes (see Fig. 1-1), whose manipulation opens the door to even more additional properties [31, 32]. Some of them, like wettability and hydrophobicity, are readily tuned through mechanical stimulus [19, 27].

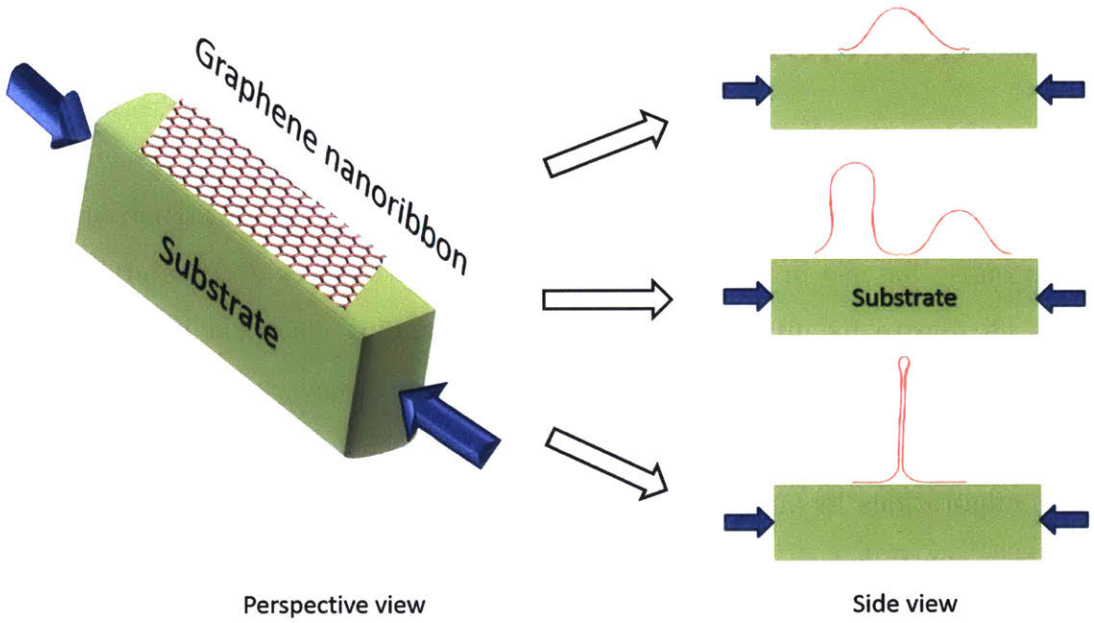

Figure 1-1: **Substrate-mediated compression of graphene nanoribbons generates different three-dimensional shapes.** Out-of-plane deformation of graphene nanoribbons is a function of the graphene-substrate interface. Shown in the right three panels are several representative shapes graphene can assume as it is being compressed. One of the aims of this thesis is to elucidate the causes of these different deformations.

Others, like electronic transport properties, can be further tuned due to twisting and compressing graphene sheets [33,34]. Additionally, graphene-based applications often need to integrate graphene into devices by adhesion to a substrate. This substrate can induce deformations on graphene due to specific graphene-substrate interactions. Thus, the above-mentioned micromechanical response of graphene to deformation, together with these substrate-induced deformations has boosted a growing body of research focusing on graphene-substrate interfaces towards emergent properties for novel applications, e.g. graphene strain engineering [35], or substrate mediated compression [19, 21, 36]. Therefore, fundamental understanding of the atomistic mechanisms underlying the deformation of graphene by the interaction with the substrate and the structure-property relation of graphene-substrate systems is crucial for a rational systematic patterning of the overlying graphene morphology at the macroscale. However, this fundamental research is often relegated for the sake of novel proof-of-concept and product-driven applied research applications.

Self-adhesion of compressed, delaminated graphene most closely resembles localized delaminated ridges of thin films compressed on a substrate, where the thin film in literature is stiffer than the underlying substrate [37]. In some cases, the substrate even deforms upwards, following the film, and into the localized ridge without any film delamination. The resulting out-of-plane protrusion also has a sharp-curved ridge tip. On the other hand, graphene forms ridges after delamination over rigid substrates with a racket-type loop at the ridge tip [17].

Graphene ridge formation during uniaxial compression progresses with delaminated buckling, growth, collapse and finally self-adhesion (stacking). The shape of delamination is not unique to graphene and previous research has studied in depth the relation between buckling shape, characteristic length scales, and onset of delamination for thin films on substrate [38]. Further compression grows the ridge more as it is fed by the surrounding planar graphene. Ridge growth can be manifest in ridge height or the tall, slender graphene protrusion can collapse on itself forming scrolls and regions of multilayer graphene at higher levels of strain [18].

This thesis analyzes a phenomenon of thin film mechanics manifest in graphene

sheets on substrate, namely delaminated buckling. When placed on a substrate monolayer graphene acts as a thin film to the extent of buckling when subjected to transverse compression. This compression force comes as a shear force across the graphene the substrate interface. Compressing the substrate allows for the compression of the overlaying graphene sheet indirectly. Compressing graphene in this way can lead to sticking and slipping on the substrate in some cases. Choice of substrate begins to play a role using this method. In this thesis, the goal is to abstract the substrate so as to only deal with a graphene sheet and model substrate without prescribing a particular substrate. What motivates this research are the potential applications of what comes next when graphene compresses as a thin film. Graphene exhibits desirable properties when compressed on substrate. A big theme in this thesis is that more can be gained by exploiting the substrate (e.g. tailoring substrate surface properties, substrate material selection) to more efficiently utilize it as an apparatus for manipulating graphene shape, rather than just using the substrate as a stage.

1.1 Research hypothesis

The key question this thesis aims to answer is why and how do observed ridges arise in graphene as it is subject to compression atop a substrate. Furthermore, can this deformation be controlled and to what extent? This work is motivated by the potential of the myriad of applications discussed in the previous section. There is sufficient work in the literature to support this research endeavor and to allow for formulation of hypotheses to answer these questions [14, 19, 27, 31, 35–37, 39–56]. The first part of this thesis will investigate the hypothesis that graphene deformation response depends on the underlying substrate in terms of corrugation wavelength and amplitude and graphene-substrate adhesion energy. Previous work has shown dependence of graphene fracture properties on graphene-substrate adhesion energy1. Also, the dependence of graphene topology on substrate roughness and corrugation has been established in the literature [41, 57–60]. The work presented in this thesis combines these two parameters, graphene-substrate adhesion and substrate roughness, to ex-

amine large three-dimensional ($>$ 10 nm) ridges in graphene. The second part of this thesis extends this work to draw a clearer picture of the mechanisms of graphene ridge formation having established two key parameters that control this mechanism. This is taken further in order to address the second key question about the extent to which this graphene ridge formation can be controlled spatially. The next section will provide motivation from the literature for addressing these questions and examine previous work to put this thesis in the context of the literature.

1.2 Literature review

The literature of graphene thin films may be categorized in many ways. A theme, however, arises: Graphene shape and form manipulation facilitates diverse functionalities [61]. Almost ironically, the 2D material is being contrived and worked into diverse 3D shapes to illicit even more desired material behaviors and responses to broaden its properties and application. This can be done with substrates present; although, substrate importance and participation varies from study to study.

Several studies have been spurred by the realization of graphene ridge formation and controlled folding and unfolding with and without a substrate [19, 27, 36, 45–52]. Many works have aimed at controlling or otherwise finding new processes to achieve hierarchical and three-dimensional configurations achievable from an initially planar graphene sheet. Modulation is key since this implies reversibility in many of the applications considering these graphene-based devices. As such, to set the stage for the thesis it is important to familiarize with the literature concerning thin film resting on substrate, specifically graphene and its integration in devices and applications forthwith. The remainder of this section will aim to provide a quick survey of this immense body of literature.

Earlier work on buckling of thin films has characterized the delamination of thin films from substrate, a key initial step in the graphene ridge formation studied in this thesis [38]. Vella et al. presented a macroscopic study of the characteristic lengths associated with thin film delamination and buckling as a function of thin

film material properties (bending stiffness, Young's modulus, Poisson's ration) [38]. Moreover, the analysis is extended to relate the interfacial adhesion energy to these characteristic length scales for a thin film allowing for measurement of the interfacial adhesion energy from the size of the macroscopically observed delaminated buckles. With knowledge of the interfacial adhesion energy, the researchers can also predict maximum stress, and therefore allowed thickness, for thin films on substrate, thereby creating a design guide for use in building stretchable electronics, for example.

Pairing thin films with substrate introduces a level of control that can be utilized for composite design. Brittle thin films can be afforded ductility when placed on a layered substrate featuring soft and stiff layers [39]. By placing the soft layer in contact with the thin film, the composite can be stretched more. This study highlights a composite design aspect of interface engineering to generate emergent properties at the composite level not possessed by the thin film alone. Thin film mechanics also elucidates the appearance of wrinkles and wrinkling patterns throughout the thin film [40–43]. This is not lost on researchers as opportunities arise to combine inherent thin film behavior with material intrinsic properties such as conductivity. One such study examines hierarchical wrinkle patterns of conducting thin films and demonstrates wrinkle pattern control can be achieved through various manufacturing processes [44]. For graphene, this opens a synergistic research opportunity to create varied wrinkling patterns and examine the emergent properties that arise.

Strain engineering can create three-dimensional hierarchical structures from a planar sheet of graphene, increasing its accessible surface area much like the cristae of mitochondria. Moreover, given graphene's exceptional conductivity it is a favorable material for future electrodes and supercapacitors. These and more examples will be explored in the remainder of this section to illustrate the need for a facile means of achieving arbitrary shapes of graphene. Many proposed and future graphene-based devices will rely on manufacturing processes borne of fundamental research on 2D material nanoscale manipulation and forming analogous to forming process of metals in contemporary technology.

Many studies focus on controlling the topology of graphene. One way graphene is

manipulated involves shock cooling with liquid nitrogen to create elastic folded sheets of graphene [45]. This method does not involve a substrate, but rather an aqueous dispersion derived from graphene oxide. After cooling with liquid nitrogen, the graphene folded structures are isolated by freeze drying the whole suspension. The result is an elastic graphene folded structure that can withstand repeated cycles of axial loading without material degradation and maintains its Japanese fan-like folds that lie on parallel axes. These folded graphene structures, however, are not reversible. Once the folds are created the graphene is fixed in that new shape, possibility deprecating the ability for tunability of any novel properties.

Another study aimed at graphene form manipulation involves heat treatment instead of cooling. Researchers have shown localized control of graphene topology through substrate heat treatment [36]. Unlike the previous cooling method to generate folded graphene structures, this study utilizes heat treatment of the underlying substrate to generate localized folded areas of graphene such that flat and folded sections of graphene can exist on one sheet. Furthermore, this process is reversible allowing the graphene sheet to be flattened after folding by again reheating the substrate. However, although reversible, this method still requires heat treatment of the substrate to achieve reversibility, which might not be amenable to or facile in integrated graphene-based devices. Both of these studies aim to create better graphene-based materials for use in electrodes and other electrical devices.

Some investigations sideline the substrate, exploring the effects of defects and mechanical torsional loading conditions to induce wrinkling in the graphene. One study showed analytically the effect of defects on graphene wrinkling patterns using von Karman plate theory [46]. The researchers further showed their graphene defect continuum model developed in this study matches very well with MD simulations they performed. Bridging continuum and fully atomistic methods creates a powerful tool for design and material behavior prediction of graphene defect effects. An obstacle remains, however, to match theory with experiment as graphene preparation and exact defect placement is still an ongoing research effort. While these approaches are appealing in theory, in practice they are tedious and less scalable for large area

graphene. However, it is clear from these studies that graphene topology can be rationally engineered and such schemes made possible for future graphene-based devices. The goal is to rationally engineer and design arbitrary shapes and structures at the nanoscale and that is what the fundamental research on graphene topology aims to understand.

More substrate and interface focused studies rely on the inherent wrinkling in graphene in addition to nucleation sites to achieve desired graphene topology control. One such study concerning better substrates for use in creating epitaxial graphene cites the inherent wrinkling of graphene in addition to the underlying substrate as key in creating higher quality (in terms of less defects, planarity) graphene [47]. This further perpetuates the paradigm of tenability of graphene; that nothing is set, and many of graphene's properties are accessible to modification. A large part of this thesis is subscribed to the idea that few properties are intrinsic to graphene when it comes to its three-dimensional geometry and that coupled with substrate, geometries that can also be hierarchical can be tailor made, for graphene and other two-dimensional materials (e.g. silicone, hexagonal boron nitride, molybdenum disulphide) [36,62–64].

Focusing more on the literature of graphene on substrate, there are also many applications and insights in literature on this topic. Graphene devices are largely electrical devices owing to its excellent conductivity (both electrical, faster electronics, and thermal, less collection of heat). It is no surprise then that care is given to the performance of future graphene devices in the context of being placed on a substrate. One such study in assessing the mechanical stability, and hence electrical robustness, of graphene compares graphene performance in two scenarios that replicating possible graphene-based devices: graphene overlying substrate, and graphene embedded in substrate [48]. Molecular dynamics simulation complemented with Raman spectroscopy are used to illustrate the stress-strain response of graphene in these two cases under axial compression. Determining critical strain levels for the onset of buckling is extremely useful for device design, as done by the researchers. Furthermore, the researchers reveal insight on how surface roughness of the substrate at the interface skews theoretically predicted critical strains from experimental findings showing that

graphene behavior is not so much intrinsic as it is dependent on boundary conditions [48], as is also demonstrated by the results in Chapters 3 and 4.

Graphene mechanical response also relates to its electrical and optical behavior, which is why strain engineering for graphene and to-dimensional material becomes so attractive. One issue, however, is fatigue lifecycle of graphene. While graphene is great in the many ways already explained, fatigue plaques almost all materials, if not all. One study set out to explore the robustness of graphene on elastomeric substrate in terms of its electrical performance [49]. A key insight uncovered by the researchers is the limit to which mechanical defects reach within the same strain range over repeated cycles. As pointed out by the researchers, this arrest of cracks is in contrast to most conductive films where onset of cracks fully degrades the material. Another study also looked into the mechanical response of graphene, but this time to its effect on graphene's optical properties. Three-dimensional graphene structures are generated and controlled through substrate-mediated compression to achieve desired photoabsorption levels in broadband photodetection graphene-based devices [50]. This study is intimately linked with a big goal of this thesis, that being controlling generated three-dimensional structures by substrate templating. It is not enough to just axially compress graphene and have it buckle out of plane [51]; this thesis aims at carefully creating arbitrary rationally designed buckling patterns and this is motivated by the nuanced application that depend on such substrate-mediated graphene out-of-plane instabilities.

Other than electrical and optical properties, surface properties that graphene can confer are also tunable through manipulation of graphene. Ridge instabilities, such as the ones that will be studied in this thesis, can arise in graphene to create superhydrophobic surfaces. Researchers first showed this trait with gold nanofilms [52], but again, graphene is also a film and it is flexible enough to produce the same effect [19, 27]. Moreover, the hydrophobicity itself can come in two flavors as seen in nature in the examples of a rose bud and a lotus leaf. On rose buds, water droplets stick on to the rose bud and do not glide off [65]. On a lotus leaf, on the other hand, water droplets immediately roll off [66]. The researchers went beyond just plac-

ing graphene on substrate to replicate these effects. This study was an example of combining origami and composite film technology with graphene-substrate interfaces and gold nanofilms to tailor the hydrophobic character of surfaces. Going beyond a graphene-substrate interface allowed the researchers to switch between two distinct effects. The substrate is usually homogenous without surface patterning or tailoring other than its own intrinsic roughness. For these studies the researchers relied on the substrate, origami folding patterns, and gold nanofilms to manipulate graphene.

These examples are few compared to the body of literature existing about graphene shape and property control. There are so many such papers that on several occasions review papers have been warranted and published concerning the topic of graphene strain engineering and its associated implications on graphene's properties. In closing this survey about varied approaches of studying graphene, the reader is directed to the review literature on the topic for completeness and reference [31,35,37,53–56]. It is important to understand the immense amount of work dedicated to the mechanics of graphene and its material characterization under different loading and boundary conditions.

1.3 Overview

This thesis is composed primarily of two parts, as outlined in Table 1.1. First, substrate-mediated compression is investigated using two parameters relating to (1) heterogeneity length scale and (2) adhesion energy scale at the graphene-substrate interface. These two parameters are varied while investigating the deformation of graphene. Second, a fracture mechanics framework is developed to analyze this substrate-mediated compression elucidating on the atomistic mechanisms that cause three-dimensional structures to form in the process of compression and suggesting possible design schemes for graphene-substrate interfaces.

Special attention is paid to a method of graphene strain engineering that indirectly compresses graphene via a substrate. With this in mind, this thesis aims at elucidating the nanoscale occurrences during compression of graphene atop a substrate.

Table 1.1: Thesis Technical Outline

Chapter	Objective	Hypotheses	Results	Impact	Gap addressed
Part 1: Ch. 3	Computational survey of graphene deformation on different substrates; warranted by a dependence of material properties on current material deformation	Graphene deformation response depends on the underlying substrate in terms of corrugation wavelength and amplitude and graphene-substrate adhesion energy	Relationship between the graphene-substrate adhesion energy and substrate roughness that defines deformed shape after finite strain	Two parameters shown to be not independent of each other with respect to final graphene shape	Delineated binary stacking versus not stacking shapes of deformed graphene
			Good agreement between continuum plate theory and simulation relating local curvature of graphene nanoribbon to potential energy of final deformed shape	Aid in future rational design of graphene and possibly other 2D material deformation shapes	Demonstrated instance of local property (curvature) affecting global material behavior (graphene deformation)
Part 2: Ch. 4	Investigate atomistic mechanisms underlying the formation, evolution, and localization of graphene ridges	Atomistic mechanism of substrate-mediated graphene deformation begins with debonding at the interface	"Pinching-in" (or squeezing) mechanism of graphene ridge formation delineated	Fundamental understanding of the evolution of graphene ridges from energy and force considerations	*A priori* reason graphene forms ridges
		Substrate mediated compression of graphene can also be used as substrate-guided compression of graphene	Rational placement of graphene ridges through tailored substrates	Tailor graphene topologies on substrates	Manipulation of substrate to incur three dimensional changes in graphene shape

Specifically, the shapes generated at the nanoscale involve delamination and folding of graphene. While it is understood some of the surface properties this imparts to the deformed graphene, it is not clear (1) the steps that happen to create the final shape, (2) the graphene-substrate interface criteria that determine the ultimate shape, and (3) the role of substrate material characterization on the deformation of graphene. The goal of this thesis is two-fold. First, to understand what happens when graphene is compressed on substrate. This is important because how the graphene deforms, and why, will help in setting the stage for future fabrication processes and possible device designs. There are various configurations graphene can take when compressed on a substrate and these grow the possible application purposes and spectrum of uses. Second, the effect of substrate through adhesion energy and surface roughness on graphene is studied to gain further insights for rational design of graphene shapes.

Chapter 2 will provide background and an overview on molecular dynamics as related to the simulations presented in this work. Chapter 3 will pertain to a broad nanoscale level sweep of the shapes achievable with substrate-mediated compression of graphene and identify possible control parameters. While experiments have demonstrated the potential applications derived from the deformation of graphene compressed on substrate, Chapter 3 aims to achieve a more fundamental understanding of how and why these deformations occurred, and what design principles can be learned to further advance the field of substrate-mediated graphene strain engineering. The second part of the thesis will pursue further a more in-depth analysis of the fracture mechanics at the interface of graphene and substrate. Chapter 4 focuses on the atomistic mechanisms that give rise to geometries observed in Chapter 3. Chapter 4 presents data and motivation for future experimental work to achieve rationally designed graphene topologies. Finally, Chapter 5 will conclude offering outlooks of this research and ways to expand on this work and take it further.

Chapter 2

Molecular dynamics

Molecular dynamics (MD) presents a well-developed tool for modeling graphene deformation as proposed in this thesis, especially in stimulating Van der Waals (VdW) type forces for the 2D material. This is because the interactions necessary to model in this thesis are covalent bonds between carbon atoms and van der Waals forces between carbon and substrate. With graphene compressed on substrate there is less chance for covalent bonds breaking. What controls the deformation are the VdW interactions between the graphene and substrate and self-interaction of nonbonded areas of the graphene. Van der Waals forces at the nanoscale control graphene shape and using molecular dynamics gives a lens to study these weak dispersive forces and their effects on graphene topology under compression. Finite element analysis, on the other hand, is not as readily equipped to properly model these dispersive nonbonded interactions. The framework of MD also provides a systematic way to quantify potential energy changes in the graphene-substrate system. Despite the limited size of system that can be modeled using MD the feature length scales associated with graphene ridge formation are small enough to allow the choice of MD as a modeling tool. MD simulations can also complement experimental work that does not always provide atomic resolution microscopy. Many researchers have likewise used the methods discussed in this chapter to study graphene using MD [67–78]. In this chapter, a brief overview will be given on molecular dynamics.

Molecular dynamics refers to a numerical solver for the equations of motion of

a set of particles. Newtonian mechanics, however, has to be adapted for a rigorous numerical implementation, which is necessary for stability and reliability of the simulations, providing accurate statistical properties of systems. The fundamental equation that needs to be solved repeatedly in simulation is Newton's second law, $\mathbf{F} = m\mathbf{a}$. Molecular dynamics needs to include time evolution in calculation of results from one point in time to the next, i.e. at every timestep. This is developed further in the next section. Time is discretized into timesteps, so that any numerical implementation needs to swiftly perform thousands if not millions of calculation for every one nanosecond of simulated time. This happens because the timestep needs to be small enough capture the highest vibrational frequency of the smallest atom in the simulation (e.g. on the order of 10^{-1} femtoseconds for hydrogen atoms).

The idea is rather attractive, then, to apply classical Newtonian mechanics on an arbitrary set of particles. Thus, molecular dynamics is grounded in a well-established realm of mechanics. The earlier challenges then were more to do with computing power than resolving the mechanics. Several key developments including more efficient algorithms and advances in computing power really bolstered MD simulations to their contemporary state.

The nuance that cannot go understated in molecular dynamics is that although the equations of mechanics allow for reversible evolution, thermodynamics, on the other hand, introduces the arrow of time. Molecular dynamics is grounded in statistical mechanics, the physics of a large number of particles that aims to derive the rules of thermodynamics as opposed to distilling them from experimental observation, which establishes the procedures and rules that govern MD simulations. There are many in-depth and eloquent treatises on this subject and the formulation of the equations of motion for MD as in Tuckerman (2008) and Bowley and Sanchez (1996). Consequently, this chapter will present a broader view of molecular dynamics, the fundamental algorithm behind it, some potentials used in this work to further motivate the choice of molecular dynamics to carry out this investigation into substrate-mediated compression of graphene, and several practical elements of MD simulations. Appendix B provides an example of a representative molecular dynamics script that

was used to do run simulations similar to those shown in Chapter 4.

Molecular dynamics is a powerful tool that allows ease of access to scales and phenomena inaccessible to conventional methods such as physical experiments. The distinction is drawn here between simulation and experimentation. For this body of work, simulations will refer to molecular dynamics simulations and experiments will refer to physical experiments done in the laboratory, for example, a tension experiment setup with a manual screw jack or a concrete creep test. Simulation can then be considered an end reached by the conduit that is molecular dynamics to translate the physical into the virtual in experimentation. However, the framework molecular dynamics provides can easily create unphysical situations in simulation when not properly checked. A classic example is presented about velocity rescaling in simulations by Harvey, Tan, and Cheatham III [81]. Their study served as a warning of the errors that can accumulate in the computation behind molecular dynamics and how these errors can lead to incorrect property calculation.

Potential functions in molecular dynamics terminology determine the interaction between atoms. It is here, during the development of these potentials, where information about the atoms in simulation, as with any transitioning point between length scales, can be lost. To understand why this is so, remember that molecular dynamics is solving classical Newtonian mechanics problems. In reality, there is a quantum nature to everything being simulated. However, molecular dynamics simulations, as such, cannot properly calculate properties that rely on electronic behavior of the atoms (e.g. electronic, magnetic, optical properties). An important nuance to note here is that the definition of a potential, a set of rules to calculate the forces that will be acting on particles in a simulation, does not preclude the types of particles simulated. Molecular dynamics then can be a misleading name because it can both be used to calculate the thermal conductivity of argon gas [82] or a game of billiards [83] (i.e. not exclusively dealing with molecules).

2.1 Time integration

Among the advances that lead to faster computation, such as use of neighbor lists and parallel computing, algorithms for efficient and fast updating of positions and velocities cannot be understated. In this section the velocity Verlet algorithm is introduced and discussed. It is quite popular because it simultaneously updates positions and velocities, not to mention its formulation will be familiar to any introductory physics student. As with any MD simulation, initial positions and velocities are set. The derivation of the velocity Verlet algorithm consists of repeated Taylor expansions of the position and velocity as functions of time. With $r_i(t_k)$, $v_i(t_k)$, and $f_i(t_k)$, denoting the positions, velocities of, and forces on particle i, respectively, and $\Phi(r_i(t_k))$ denoting the position dependent potential function, the velocity Verlet scheme can update positions and velocities simultaneously with known initial positions and velocities and a given potential function.

$$r_i(t_0+\Delta t) = r_i(t_0) + v_i(t_0)\Delta t + \frac{1}{2}\left(\frac{f_i(t_0)}{m_i}\right)(\Delta t)^2 \tag{2.1}$$

$$v_i(t_0+\Delta t) = v_i(t_0) + \frac{f_i(t_0)}{m_i}\Delta t + \frac{1}{2}\ddot{v}_i(t_0)(\Delta t)^2 \tag{2.2}$$

$$\ddot{v}_i(t_0)\Delta t = \frac{f_i(t_0+\Delta t)}{m_i} - \frac{f_i(t_0)}{m_i} \tag{2.3}$$

$$v_i(t_0+\Delta t) = v_i(t_0) + \frac{1}{2m_i}\left[f_i(t_0) + f_i(t_0+\Delta t)\right]\Delta t \tag{2.4}$$

where $f_i(t_k) = -\nabla\Phi(r_i(t_k))$. First the positions are updated after $f_i(t_0)$ is evaluated , $r_i(t_0+\Delta t)$, then $f_i(t_0+\Delta t)$ is evaluated in order to update the velocities, $v_i(t_0+\Delta t)$.

2.2 Ensembles

The way molecular dynamics is able to provide any relevant physical information is based on the idea of ensembles. An ensemble is a fictitious set of microscopic states that all have the same thermodynamic macroscopic state. For example, given a set of atoms in an adiabatically isolated box of fixed volume, there is a multitude of

microscopic states this box can be in that would all correspond to that box having the same macroscopic state (e.g. same measure of pressure or temperature). Molecular dynamics, however, at any given timestep only samples one microscopic state at one point in time (timesteps do not overlap). There are many microscopic states in a given ensemble. To calculate properties for a system from its microscopic states it would not be enough to do so based on one snapshot of one microscopic state. Instead, property calculation is done by averaging over many microscopic states. This can be done in two ways. Monte Carlo approach averages over many snapshots of different microscopic states with the same ensemble, while MD does time averaging of all the microscopic states sampled in a simulation. It turns out by the ergodic hypothesis that an ensemble average and a time average, when converged, both give the same result. The two averaging schemes are equivalent. The ergodic hypothesis explains why Monte Carlo and a Molecular Dynamics schemes are equivalent in terms of their thermodynamic properties under a given ensemble.

An ensemble is a collection of fictitious microscopic copies that could pertain to the same macroscopic observables. These copies are not independent, however, and their similarities actually identify the ensemble. For example, an ensemble whose copies have the same number of particles (N), volume (V) and internal energy (E) is termed the microcanonical ensemble and is actually the *de facto* ensemble in simulations if no other modifications are made to the time integration scheme (i.e. velocity Verlet algorithm). In the microcanonical (NVE) ensemble every copy of the microscopic state has the same number of particles, volume, and energy. The same applies to other common ensembles used in simulation such as the canonical, grand canonical, and isobaric-isothermal ensembles. In the canonical ensemble, particles number (N), volume (V), and temperature (T) are kept the same across all realizations of the ensemble. The canonical ensemble was actually used for most simulations in this thesis. The grand canonical and isobaric-isothermal ensembles are termed μVT and NPT, respectively, where μ and P refer to the system chemical potential and pressure, respectively.

2.3 Molecular dynamics software

A molecular dynamics simulation needs to take in as an input a list of commands the simulation will perform and a set of initial positions and velocities. Usually this consists of an input script that can specify the initial velocities and a data file that contains the coordinates for the initial geometry. A widely used molecular dynamics software package that is also used for the work presented in thesis is Large-scale Atomic/Molecular Massively Parallel Simulator (LAMMPS) [84]. As with any software undertaking it is crucial to know what that software can and cannot do. This is even more important with molecular dynamics because what is to be expected from simulations will be limited by the code used to run them. For example, the input script used to run simulations with LAMMPS can only invoke commands that are built-in to LAMMPS. Over the years the command list has grown and even some user-defined commands have been incorporated, but it still remains the best practice to learn what these commands are and how they might be used in a simulation. This is how the commands available in a software package can determine how useful simulation results will be; the commands need to encompass a sufficient set of basic actions to simulate user-defined models and be able to extract meaningful results and data. Modeling and simulation can be considered a study in deconstruction of the components of a complex system and isolating key facets of interest to target desired features of study.

2.4 Fundamental molecular dynamics algorithm

The main idea behind a molecular dynamics simulation is to observe the evolution of a set of particles with given initial positions and velocities over a finite timescale. Then, the approach is to observe the behaviors of particles under certain macroscopic settings, while also being able to apply additional constraints on the particles or the entire system to test how they deform or fail under these specific conditions. The simulation runs computing the forces on the particles at every timestep and updating

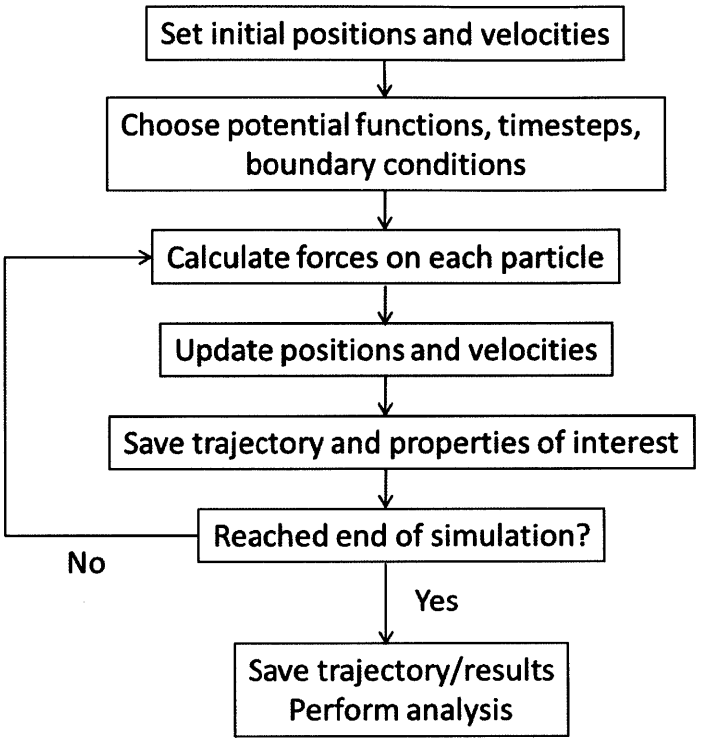

Figure 2-1: **Molecular dynamics flowchart.** The first step is to initialize a simulation by providing starting positions and velocities. Afterwards a simulation can just run indefinitely once a potential is provided. Depending on user interest the simulation can involve more complicated boundary conditions or just stay approach and stay at equilibrium. The simulation is done when the user terminates either by setting a maximum number of timesteps or the simulation can crash in which diagnostics are in order to resolve the issue. The goal at the end is to have accrued enough desired data for the properties of interest to proceed with the study.

the positions and velocities (e.g. velocity Verlet algorithm). Initialize, run, terminate, and analyze. Often this is depicted in a flowchart as in Figure 2-1. The flowchart help gives a big picture view of what it means to run a molecular dynamics simulation, and is often instructive for beginning and experienced molecular dynamicists.

2.5 Potential formulations

Potentials define particle interactions within a molecular dynamics simulation. While it may be instructive to refer to potentials by analogy in common vernacular, a grounding technical treatment is necessary to understand how they work and why

they are needed. This section will delve more into the technical aspect of potentials, their functional forms and their implementation. For this thesis, two potentials will be highlighted as they are the two main potentials that will be encountered in the following chapters, the Morse and Adaptive Intermolecular REactive Bond Order (AIREBO) potentials [85, 86]. Discussing these potentials will speak to other potentials and garner a deeper understanding for their role in MD. Furthermore, these potentials will be compared to each other highlighting their advantages and disadvantages and their differences. It is oftentimes useful to be aware of as many potentials as possible when one decides to run a MD simulation in order to maximize efficiency. After all, being economical with computational time will always be key even as computers get better and fast; that is how progress is pushed forward and how technology still becomes better and faster.

This thesis aims to present simulations done with graphene as the key material. The molecular dynamics simulations presented, thus, include potentials adequate for the simulation of graphene. Two different potentials are used over the course of this thesis. In the next two sections each will be discussed in turn, the Morse and adaptive intermolecular reactive empirical bond order (AIREBO) potentials [85–88]. Their origins, uses, and functional forms will be expounded on and when appropriate their merits contrasted. It is always essential to understand the power and drawbacks of the tools for any purpose, and the same rings true with molecular dynamics simulations of particles. Furthermore, elaborating on these two potentials serves as case studies of potentials, and so, simultaneously gives insight and comprehension of what a potential (or force field) is and can be in the realm of molecular dynamics.

2.5.1 Philip M. Morse potential

The Morse potential, named after Philip M. Morse, and derived as a solution to the Schrödinger equation of the motion of diatomic molecules such as BeO, AlO, C_2, CN, CO, F_2, I_2, N_2, NO, O_2, and SiN to name a few. Unlike AIREBO the Morse potential was analytically derived in Morse's original paper in 1929 [85]. This potential was used as part of a suite of potentials to describe the carbon-carbon

bonding and nonbonding interactions in this study. The Morse formulation was used specifically to simulate the covalent bonding network in graphene between pairs of carbon atoms. The main attraction of this implementation is its higher computational efficiency compared to a reactive potential, such as the one to be described in the next section. Furthermore, the nature of the simulations in this study did not warrant a reactive potential formulation as no bond breaking or forming is anticipated during buckling of graphene. Moreover, to see this buckling no bond breaking or forming was necessary. Simulations that are concerned with fatigue, for example, would, on the other hand, need to use a reactive potential to see crack initiation. The Morse potential from the original paper had the form:

$$\Phi_{\text{Morse}}^{\text{orig}}(\mathbf{r}) = A - D + D\left(1 - e^{-\alpha(\mathbf{r}-\mathbf{R})}\right)^2 \tag{2.5}$$

The term A, meant to zero the potential with respect to the neutral molecule was later set equal to D, the depth of the potential well, since the zero of the potential is arbitrary and relative energy differences are more meaningful than absolute values. The most commonly used form of the Morse potential, thus looks like this:

$$\Phi_{\text{Morse}}(\mathbf{r}) = D\left(1 - e^{-\alpha(\mathbf{r}-\mathbf{R})}\right)^2 \tag{2.6}$$

where α arises from solving the Schrödinger equation with Morse's original trial function and represents a stiffness parameter in the potential, and R represents the equilibrium bond distance, each of which each has to be fit from experimental data or from the more involved class of quantum mechanics simulations. Plots of the Morse potential with different values of D and α (with R set equal to 1.3 Å), help to demonstrate their effects on and meanings in the potential (Fig. 2-2).

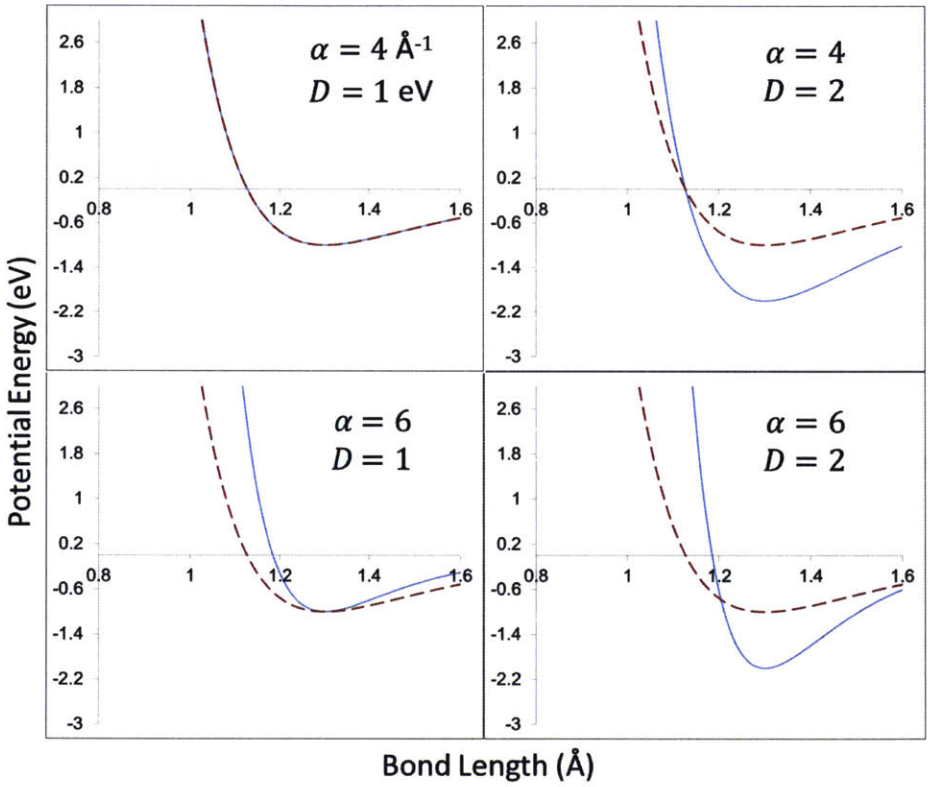

Figure 2-2: **Morse potential parameter sensitivity.** The Morse potential is plotted without zeroing the potential for easier visual comparison. It is clear that D represents the depth of the potential energy well and α represents the steepness or stiffness of the potential energy function. The equilibrium bond distance is set to 1.3 Å for all plots; the minimum energy occurs at the equilibrium bond length. Dashed lines are the same original parameter set of (α,D)=(4,1) and are reproduced in all panels for reference.

2.5.2 Adaptive intermolecular reactive empirical bond order potential

One of the potentials used in this thesis is the adaptive intermolecular reactive empirical bond order (AIREBO) potential, developed for hydrocarbon systems [86–88]. Graphene is made up entirely of carbon and is not functionalized in this study so that AIREBO is well suited for modeling the carbon atoms in a graphene sheet [77, 78, 89–92]. Since AIREBO is a reactive potential, as will be discussed in this section, it also means only the initial geometry is required to start a simulation with no need to specify information about the system, such as enumerating bond and dihedral angle lists. Even though no failure of graphene is anticipated in this study AIREBO provides a benchmark for validation of the Morse-based potential used to model the graphene sheet in simulation. In this study AIREBO was prohibitively computationally expensive to perform the systematic sweep of graphene deformation shapes presented in Chapter 3. Chapters 3 and 4 will go into more detail about the modeling of graphene.

AIREBO can be readily and succinctly, although deceptively concisely, described and explained by its name. First, consider the bond order character of this potential. Bond order as put forth by Abell can be related to coordination number of an atom in a molecule [87]. This was later expounded on by a set of experimentally derived parameters by Tersoff, creating an empirical bond order description of a specific number of elements [88]. Roughly bond order can be thought of as a continuum of bond strength and inverse of atom coordination number. Triple bonds are stronger and shorter than double bonds; the bond order of triple bonds is higher than that of double bonds. Bond order can at the same time inform on the hybridization of carbon atoms being simulated, and so a classical implementation greatly decreases computational cost. The downside, of course, is a drop in accuracy, which is remedied by fitting procedures and a comprehensive enough parameter test set.

Brenner used the Abell-Tersoff analytic formulation of bond order coupled with a parameter set of hydrocarbons to create a reactive empirical bond order (REBO)

that could be used to simulate breaking and forming of covalent bonds to model chemical vapor deposition (CVD) of diamond [87]. The benefit of a reactive potential such as REBO is that system topology and connectivity is already built-in. The data file to run a simulation need not specify bond lists or dihedral angles, for instance. However, this means the onus is shifted on the user to make sure the potential is up to the task of modeling the system of interest accurately enough. REBO, for example, only considers nearest neighbor interactions with a slight modification afforded by the many body information embedded in the bond order correction term of the potential. This is best exemplified by examining the functional form of the first generation REBO potential,

$$E_{ij}^{REBO} = V_{ij}^{R} + b_{ij} V_{ij}^{A} \tag{2.7}$$

where V^R and V^A are the repulsive and attractive contributions to the potential, respectively. Each of these contributions in turn has a distance dependency that switches the potential on for nearest neighbors only, therein giving REBO its short-ranged characteristic. The bond order term, b, weights the attractive contribution based on the bond order of the nearest neighbors, i and j, taking into account the local environment (this includes coordination number, bond angles). This allows double bonds for example to be stronger than single bonds in the REBO framework. REBO utilizes this bond order term to circumvent costly quantum mechanics calculations using only the coordinates of the atoms. The reader is referred to Brenner's original paper for full details of the REBO implementation [87].

A solid network system like diamond might be adequately simulated using the REBO potential, but even in covalent networks repulsive contributions from the lattice still play a small role. The short-ranged character of REBO leaves it unfit for simulation of liquid hydrocarbon chains, for example, where non-bonded interactions can play a pivotal role [93, 94], even more so for 2D materials such as graphene [63, 64, 95, 96]. Thus, one of the biggest drawbacks of the REBO potential is its lacking characterization of intermolecular, as opposed to intramolecular, inter-

actions. Covalent bond breaking and forming is a cornerstone of REBO, and so any update to this potential would have to work to maintain its reactive capability. An intermolecular REBO would have to still be able to capture the strength of covalent bonds while at the same time include extra attractive and repulsive forces in a many-body local environment. All while only relying on the geometry of the system and not resorting to quantum mechanical calculations, whose computational cost motivated a classical reactive potential in the first place. Stuart, Tutein, and Harrison incorporated a Lennard-Jones (LJ) term into the AIREBO potential to introduce distant (more than 2 atoms between) neighbor interactions [86].

The final piece of the AIREBO puzzle is making the potential adaptive. A reactive potential means atoms can move positions and chemical bonding can change. Including intermolecular interactions complicates things with a reactive potential because now not only do nearest neighbor bonding interactions need to be updated, but also nonbonded neighbor interactions. The potential needs to address many-body effects on both bonded and nonbonded neighbor interactions. To address this AIREBO incorporates a suite of switching functions and bond weighting terms.

The Lennard-Jones potential is a ubiquitous, computationally tractable potential commonly used to model nonbonded interactions such a van der Waals dispersive forces. The form of the Lennard-Jones 12:6 potential used in the AIREBO potential is

$$V_{ij}^{LJ}(r_{ij}) = 4\epsilon_{ij}\left[\left(\frac{\sigma_{ij}}{r_{ij}}\right)^{12} - \left(\frac{\sigma_{ij}}{r_{ij}}\right)^{6}\right] \tag{2.8}$$

where the only two parameters are ϵ, the potential energy well, and σ, the point where the potential energy crosses zero and characteristic length scale related to the equilibrium bond distance through the relation $r_e q = 2^{\frac{1}{6}}\sigma$. To ensure this added term does not tamper with the effectiveness of the original REBO potential LJ interactions are gated by three separate switching functions which are further weighted by bonding between atoms. Bond weight ranges from 0, nonbonded, to 1, bonded, for pairs of atoms. The three switching functions check for:

1. Connectivity: LJ interactions are turned off for next nearest neighbors and closer. Neighbors farther than this are weighted by their bond dissociation. LJ interactions are partially turned on for pairs of atoms sharing three of fewer bonds with intermediate bond weights in the range (0, 1).

2. Distance: Minimum and maximum cutoffs for the LJ term are defined creating shells of allowed interaction regions around atoms to include nonbonded interactions in the AIREBO potential.

3. Bond Order: AIREBO still has to maintain its reactivity. If two atoms are within bonding distance the LJ term is turned off to avoid the repulsive effect that would create an artificial barrier for bond forming. However, if the two atoms are very far apart the bond order switching function is set to zero and only connectivity is checked to see how much the LJ term should be turned on if at all.

In effect, the LJ term is turned on between atoms that that are connected by two or more atoms. These switching functions are separate from the bond weighted distance switching functions of the original REBO potential that checked whether or not pairs of atoms were in range to create a bond and if bonded pairs of atoms had moved too far from their allowed stretched bond length. With these rules set there is one more addition to REBO to get the full AIREBO. AIREBO also adds an additional torsional interaction term to account for rotation of bonded atoms about their bond axis.

The adaptive intermolecular reactive empirical bond order (AIREBO) potential is as stated. The discussion first starts out with the bond order (BO) formulations of Abell and Tersoff, to be utilized later by Brenner to create the first generation reactive empirical (RE) bond order potential for simulating chemical vapor deposition of diamonds. In an effort to expand on the utility of REBO to include other hydrocarbons beyond systems that are primarily governed by covalently bonded networks, Stuart, Tutein, and Harrison [86], and later Brenner et al. [88], included distant neighbor interactions to the REBO potential. This modification allowed REBO to better

simulate intermolecular (I) interactions beyond covalent bonds. Finally, a series of switching functions and bond weighting functions allowed the AIREBO potential to be adaptive (A) as bonds formed and broke and atoms moved from their equilibrium positions. The AIREBO potentials further received an update when its performance under high pressure was less than desirable as compared to quantum mechanics calculations. Thus, AIREBO-M is proposed by O'Connor, Andzelm, and Robbins in 2014 [97], substituting the Lennard-Jones term modeling non-bonded interactions with a Morse potential term. The evolution of AIREBO serves as a case study in potentials in molecular dynamics and stresses their bridging role between the physical and the virtual.

THIS PAGE INTENTIONALLY LEFT BLANK

Chapter 3

Compression deformation regimes of graphene on substrate

The work presented here was published in:

- **T. Al-Mulla**, Z. Qin, and M. J. Buehler. Crumpling deformation regimes of monolayer graphene on substrate: a molecular mechanics study. *Journal of Physics: Condensed Matter*, 27(34):345401, 2015.

3.1 Introduction

Many examples of graphene devices and applications have been surveyed in Chapter 1. However, to facilitate this growth and expansion of graphene applications it is necessary to gain fundamental understanding of graphene's mechanical instabilities. This chapter focuses on buckling, delamination, and out of plane configurations of graphene compressed on substrate. Through these mechanical instabilities graphene can be tuned to achieve desired transport properties [60, 99, 100] and pave a path to create arbitrary three-dimensional nano-architectures.

Passive configurations of graphene on substrate, which are caused by laying graphene on substrate, have already been studied and heuristic models have been generated in predicting graphene conformation at the interface [57, 58, 101]. These studies show that substrate surface dimensions and interfacial adhesion energy determine

the transition points between graphene conforming to the substrate topology and graphene lying flat on the substrate surface. Determining graphene conformation on substrate allows for designing and predicting graphene electrical device performance as graphene's electrical properties are directly linked to its geometry [102–105]. In contrast, active configurations of graphene, which are achieved by mechanical compression of the graphene after placing it on a substrate, for example, leads to out-of-plane geometries [19]. Graphene ridge formation in particular, is a controllable, active, mechanically accessible shape of graphene already shown to have applications in flexible capacitors for energy storage [21]. It is an attractive application by using different graphene configurations as multifunctional surfaces. However, to reach this goal and be able to quantitatively control the configuration by knowing the critical condition for structure transitions requires fundamental understanding of graphene deformation under different mechanical and boundary conditions but not merely the mechanics of the graphene *per se*.

The aim of this chapter is to investigate the critical conditions for graphene ridge formation with different characteristic configurations by using full atomistic molecular dynamics simulations. Uniaxial compression tests are simulated to study the out-of-plane behavior of single layer graphene and identify and characterize the detaching mechanisms of graphene ridge formation on a substrate as seen in experiments. The effects of interfacial adhesion energy and substrate surface topology, parameters inherent to any material-substrate interface, on graphene ridge formation atop a substrate are systematically investigated. This will pave the way for future applications by converting graphene into three dimensional folded structures with functional, mechanical and electronic properties according to design.

3.2 Methods

Graphene ridge formation is modeled based on experimental and simulation work done compressing graphene sheets on a pre-strained elastomeric substrate [19]. Molecular dynamics simulations are carried out using the Large-scale Atomic/Molecular Mas-

sively Parallel Simulator (LAMMPS) software package [84]. The model system is made up of a fully atomistic monolayer graphene sheet 1,000 by 100 Å and an idealized substrate. The substrate is modeled as an impenetrable boundary condition on which the graphene rests. Furthermore, different substrates are generated by introducing different patterns of particles on the surface on this impenetrable wall. These particles interact with the graphene sheet via a Lennard-Jones potential. Multiple simulations are carried out varying only two parameters to identify their effect on the final graphene sheet shape after compression. These two parameters are the overall interfacial adhesion energy and the length constant that describes the periodic adhesion strength that takes the substrate surface roughness into account for the substrate models.

3.2.1 Model of the graphene sheet

The fully atomistic graphene is modeled using a Morse potential based force field developed for carbon nanotubes [106]. This work adopts the same simulation setup using carbon-carbon bond interactions characterized by a Morse potential, harmonic dihedral angle potential, 12:6 Lennard-Jones (LJ) potential, and cosine-squared harmonic angle potential (see Table A.1). The choice of potential was to increase computation tractability and reduce computation time for larger system sizes. Comparisons between this suite of potentials and the adaptive intermolecular reactive empirical bond order (AIREBO) [86] are in well agreement and so the faster Morse potential based force field is implemented.

Validation of the more efficient set of potentials is carried out by indentation of a simply supported sheet of graphene as shown schematically in Figure 3-1(a). Indentation tests are performed on various graphene sheet sizes with various sizes of indenters. The comparison of the two force fields shows excellent agreement despite the fact that the AIREBO potential shows larger force and stiffness under extreme large tensile deformation before rupture, as shown in Figure 3-1(b). Such difference arises because the Morse potential based force field does not take bond-order change and bond rupture into account during deformation but AIREBO does, yielding differ-

ent reaction force at larger tensile deformation. However, such extreme large tensile loading condition cannot happen during compression before or after ridge formation because of the atomically thin nature of graphene that places all the carbon atoms on the neutral axis in bending. Therefore, the Morse potential based force field is a proper tool that provides efficient and sufficient accuracy for the current study.

3.2.2 Model of the substrate

Modeling the coarse grained substrate was done by introducing a composite substrate made up of a potential wall and embedded bead particles that both interacted only with the graphene sheet and not with any other part of the substrate. The potential wall is a 9:3 LJ wall. Earlier work has shown this choice of a potential was suitable for a virtual wall and fluid interaction [107] and as a substrate for graphene in simulations [19]. Just the wall on its own, however, would always only model the substrate as perfectly smooth. This will be shown to only ever lead to one mode of deformation of graphene. Embedded beads in the substrate are introduced in order to compensate for this. Beads are modeled as discrete particles that have a 12:6 LJ interaction with the carbon atoms of graphene. Varying the interfacial adhesion energy in a simulation was done by setting the LJ interaction between beads and the graphene sheet. The arrangement of the embedded beads is changed as a means of changing the substrate surface topology.

Beads in the substrate are arranged in rows running lengthwise perpendicular to the direction of the lateral compression in the simulations (see Figure 3-2). Every row is composed of 233 beads where a row can be thought of as a discretized nanowire on the substrate. This setup creates a bead spacing, what can be thought of as spacing between adjacent nanowires [57], parameter in the direction of compression (the x-direction), which is varied for different simulations to investigate the effect of substrate surface properties on the final shape of graphene after deformation. The beads are points that interact only with the carbon atoms through a Lennard-Jones 12:6 potential. All beads are identical in their interaction with the graphene in this way. The only difference is the position of each bead. Their effective size is a sphere

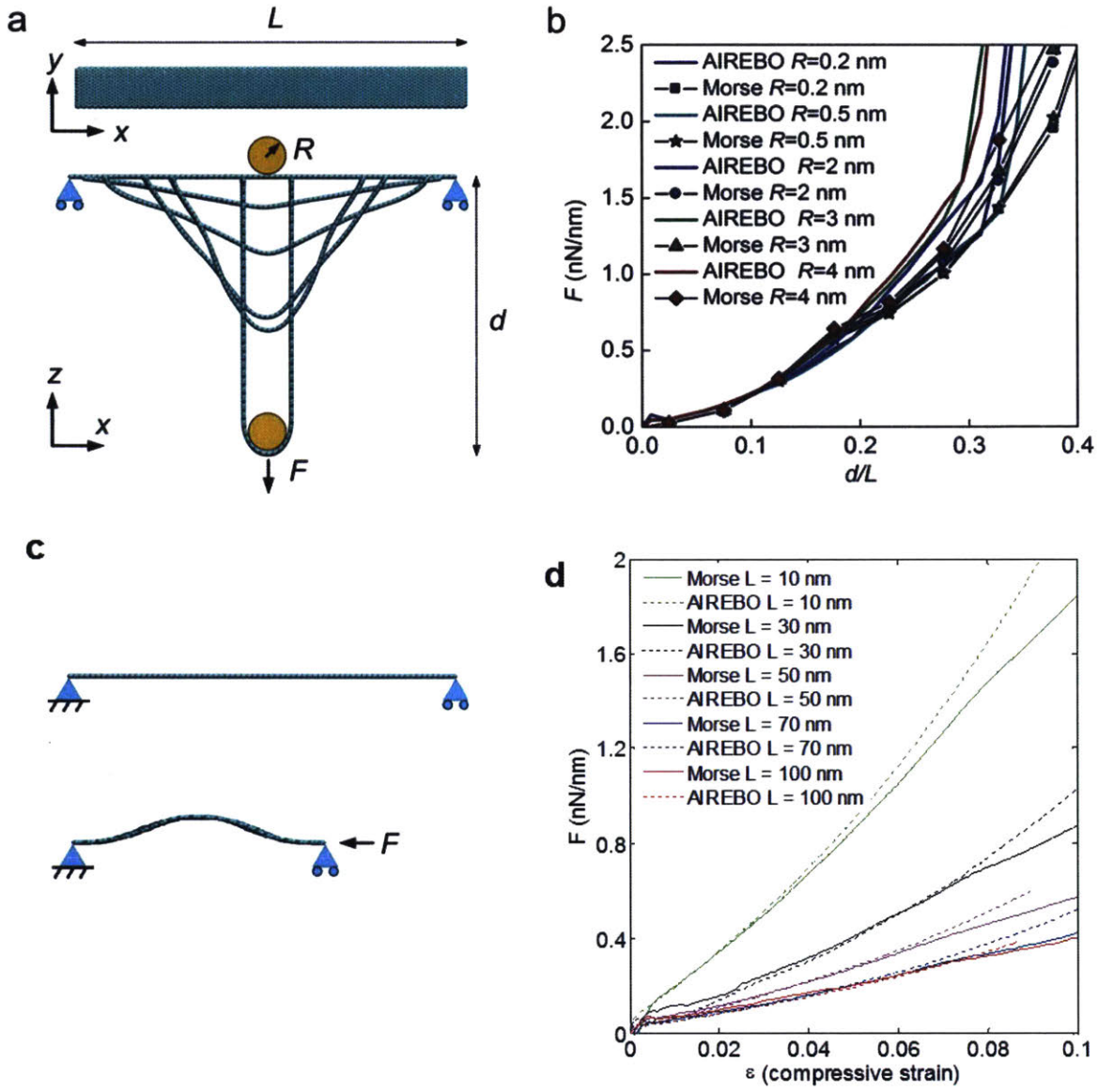

Figure 3-1: **Validation of the force field used for carrying out the simulations.** (a) Schematic of the test simulations run to compare the AIREBO and Morse potentials. Simply supported edges are achieved by fixing a line of carbon atoms on either side of the graphene sheet. Compared to AIREBO the Morse potential is in well agreement for (b) indenter radii less than 30 Å. The maximum effective radius of the substrate beads used in simulations is 10 Å, so the Morse potential, which is more efficient in this case, is chosen over AIREBO for this study.

of radius 10 Å, while the equilibrium separation between a bead and a carbon atom is set to be 3.76 Å. This is done to introduce an out of plane heterogeneity compared to the equilibrium distance between the graphene and the 9:3 LJ potential wall of 3.35 Å.

The interfacial adhesion energy is set through the LJ energy parameter of the interaction between beads embedded in the substrate and carbon atoms in the graphene sheet. Different energy values are used corresponding to interfacial adhesion energies ranging from 50 to 2,500 mJm^{-2} (see Table A.2). Choosing to use the same LJ energy parameters means different spacing configurations will have different total interfacial adhesion energy values. This scheme keeps adhesion energy per bead approximately the same for different nanowire spacing simulations. Small differences arise due to edge effects. This was done as opposed to keeping the total interfacial adhesion energy constant and varying the beads from simulation to simulation since this would generate a different set of beads for different spacing values. The results actually justify using identical beads as the jump transition between different deformation regimes occurs in the same range of per bead interfacial adhesion energy (0.3-0.5 mJm^{-2} per bead), not total interfacial adhesion energy.

3.2.3 Simulation setup

Interfacial adhesion energy and substrate topology is varied across different simulations to delineate the phase space of possible deformed graphene configurations. Bead spacing is varied by increasing the number of rows of beads on top of the substrate. For example, a nanowire spacing of 500 Å would correspond to two rows of beads for a graphene sheet of length 1,000 Å. Interfacial adhesion energy is changed through the 12:6 LJ interactions between carbon atoms and bead particles on the substrate. It is only these two parameters that are changed in running simulations to identify the final deformed shape of graphene.

Molecular dynamics simulations with 100 nm by 100 nm graphene sheets without heterogeneity in the substrate and biaxial compression of the graphene-substrate interface have been reported [19]. By comparison, the graphene nanoribbons in this

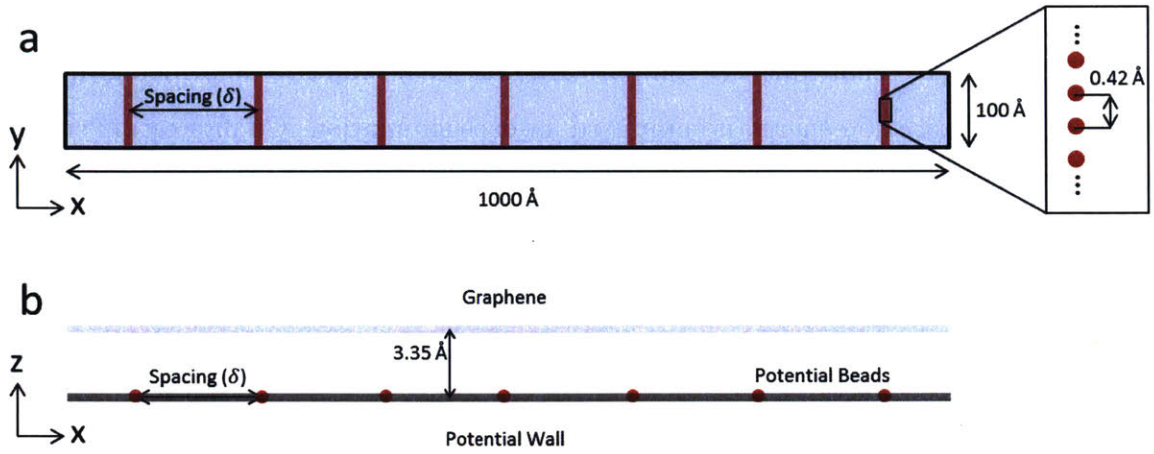

Figure 3-2: **Setup of the system to model graphene ridge formation.** (a) A graphene sheet is overlain on a composite substrate. (b) The substrate is made up of a Lennard-Jones (LJ) 9:3 potential wall embedded with LJ 12:6 potential beads to model heterogeneity in the substrate as opposed to a perfectly smooth surface. There is no interaction among beads and the beads are treated as rigid bodies. Displacement control is used to apply compression at a strain rate of 0.2 ns^{-1}. The parameters varied in different simulations are the nanowire spacing (δ) and interfacial adhesion energy.

study have an aspect ratio of 10 on a tailored substrate and focus on uniaxial compression. This allows systematic exploration of a wider range of initial conditions to distill key parameters that affect graphene deformation. While heterogeneity is introduced through the nanowire-like beads in the substrate, this is still an idealization [108]. Various bead spacing values are, thus, implemented to compensate for this discrepancy. A small system size allows for greater exploration of phase space, but is also limited in its own regard. Experiments observe ridge formation at the micron level, but simulations enable observation it at the nanometer level with extremely high resolution.

Compression of the simulation box occurs at a very high, simulation-accessible strain rate of 0.2 ns^{-1}. All beads are modeled as rigidly embedded in the substrate and move with the substrate as it deforms. Time integration is performed in the canonical ensemble at a temperature of 300 K. Clamped boundary conditions are applied on the left and right edges of the graphene sheet and keep the top and bottom simply supported. Visual Molecular Dynamics (VMD) was used to visualize the

simulation trajectory and AtomEye was used to map simulation data on the graphene sheet [109,110]. To quantitatively compare different final shapes of deformed graphene sheets the configuration energy is computed for each simulation. Configuration energy is taken to be the difference in potential energy of the graphene sheet from the final deformed shape and the initial equilibrated sheet. The final deformed shape is taken to be after 23% strain in compression is applied to the substrate.

3.3 Results and discussion

A set of simulations are performed with different bead spacing and interfacial adhesion energies. Interfacial adhesion energy is varied from 50 to 2,500 mJm^{-2} and nanowire spacing (δ) is varied from 71.4 to 500 Å (14 to 2 nanowires on the substrate surface, respectively) [57]. Typical values of interfacial energy range in the hundreds of millijoules per square meter, from 450 mJm^{-2} between graphene and silicon dioxide, and 1,000 mJm^{-2} for copper-graphene interfaces [111,112]. The minimum nanowire spacing is set sufficiently larger than both the C-C bond length (1.42 Å) and the longest distance across a graphene aromatic ring (2.84 Å) in order to avoid confounding size effects. Results show two distinct shapes that graphene assumes upon compression, with a distinct transition in between that is a function of the interfacial strength and roughness of the substrate, as shown in Figure 3-3.

Such an out of plane deformation of graphene sheet can occur in one of two ways. Graphene can either form ridges or buckle out of plane. In both cases the deformation is associated with delamination between graphene and substrate. Although graphene ridge formation has been studied before [20], the focus here is on a particular uniaxial compression based on previous work [19]. Graphene ridge formation is defined here as buckling followed by self-adhesion, or stacking, of the buckled regions of the graphene sheet, which provides a more stable folded structure than purely buckled ones that strongly depend on the boundary confinements.

The simulation results quantify how interfacial adhesion energy and substrate bead spacing define the initial conditions imposed on the graphene sheet that determine

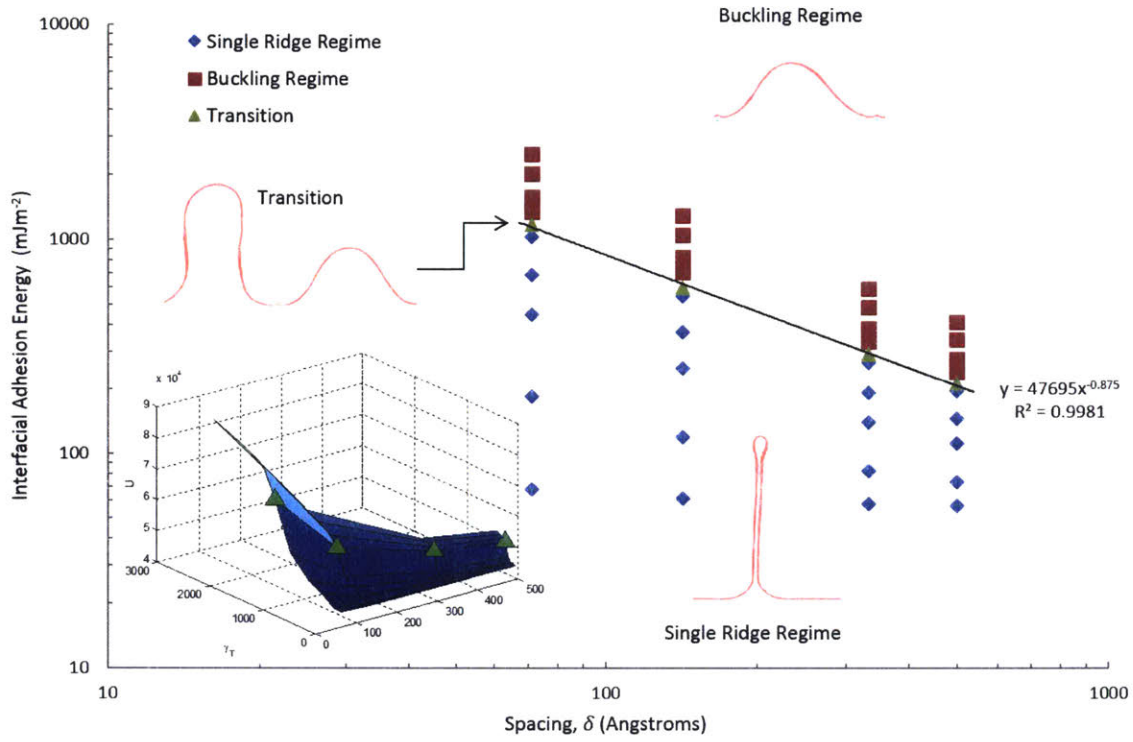

Figure 3-3: **Phase diagram of deformation regimes** showing finite range of shapes graphene can form during compression for a given range of interfacial adhesion energies and substrate surfaces. Adhesion energy of the graphene-substrate interface controls when graphene ridges as opposed to buckling out of plane without self-adhesion for a given substrate surface. Bead spacing in the composite substrate determines the onset of deviation from the single ridge regime. The higher the beads spacing is, the lower the adhesion energy allowance for the single ridge regime. Power law relating the two parameters is fit to $\gamma = 47695\delta^{-0.875}$, where γ is the interfacial adhesion energy. Inset: Representative profile view of the various shapes observed for graphene during compression to 23% strain. Inset bottom left: Three-dimensional view showing all parameters considered for this study, configuration energy, interfacial adhesion energy, and bead spacing. Transition points are shown as green triangles.

whether the graphene will form ridges or buckle (see Figure 3-3). For a given bead spacing a graphene sheet will exhibit only ridge formation up to a critical value of adhesion energy, above which the graphene sheet will also start to exhibit buckling. Coexistence of ridges and buckled regions is observed for different values of bead spacing (see Figure 3-4(a)), but the trend of buckling appearing above a critical adhesion energy is consistent for all substrates regardless of bead spacing. In the phase space of total interfacial adhesion energy and bead spacing, there is a curve that delineates the transition point at which buckling begins to occur in the graphene sheet.

Ridge formation and buckling are not only morphologically distinct, but also energetically distinct. The least energy configuration dictates the shape of a compressed graphene sheet. Buckling only becomes the mode of deformation after sufficient energy in the form of interfacial adhesion energy is introduced into the system in this model. As the interfacial adhesion energy is increased across different simulations, the evolution of configuration energy due to the deformation of graphene, from the original flat graphene sheet to its deformed shape, shows a smooth increase from the ridge creation to buckling regimes. As the configuration energy increases with interfacial adhesion energy, the deformation mode switches from creating ridges to buckling.

The same trend occurs for all instances of bead spacing. However, bead spacing affects this change in configuration energy in two ways. Bead spacing determines the two deformation regimes of graphene (see Figure 3-5). Higher bead spacing systems are more likely to exhibit concurrent regions of buckling and ridges, whereas low bead spacing systems will have either only ridges or only buckling (see Figure 3-4(a, c)). Formation of ridges causes the configuration energy to decrease due to self-adhesion in the ridges. For low bead spacing, the interfacial adhesion energy is necessarily higher due to the increased number of beads in the substrate. Higher interfacial adhesion energy and the absence of graphene ridge regions lead to a larger difference in the configuration energy of the two regimes of deformation.

There are two deformation regimes for any given bead spacing. More illustratively,

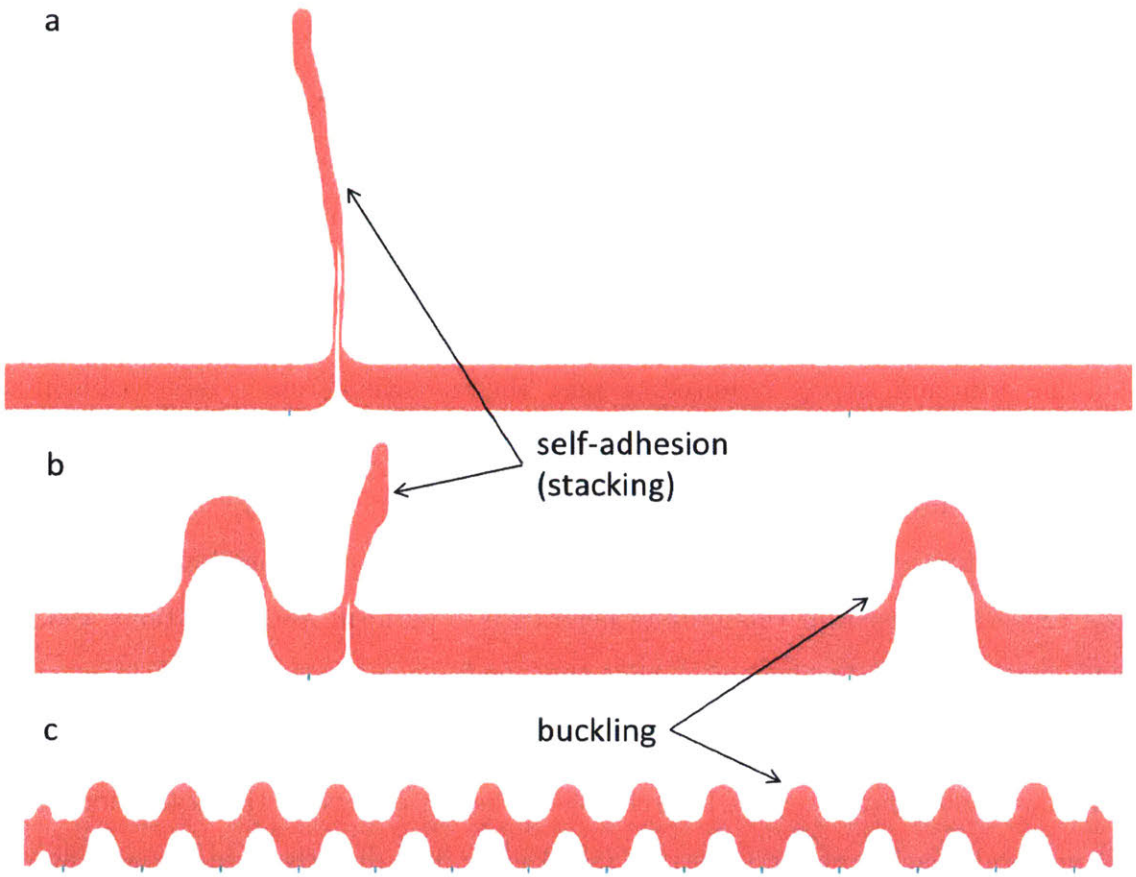

Figure 3-4: **Representative shapes of graphene nanoribbon deformation configurations after uniaxial compression on substrate.** (a) Single ridge regime occurs for all substrates independent of the bead spacing as long as interfacial adhesion energy is below the critical value, which is a function of the bead spacing (500 Å, and 111.4 mJm^{-2} shown here). (b) For high bead spacing above the transition point concurrent ridge creation and buckling can occur (500 Å and 276.4 mJm^{-2} shown here). (c) Above the transition point for low bead spacing only buckling is observed (71.4 Å and 1579.2 mJm^{-2} shown here).

the analysis is extended to consider two extreme cases. The first case is that of infinite bead spacing. Infinite bead spacing means there are no beads on a perfectly smooth substrate. The second case is that of zero bead spacing, which is equivalent to having an infinite number of beads. This also would yield a perfectly smooth substrate. Naturally, it would then be expected that both cases yield a similar deformation regime because both reproduce the perfectly smooth substrate, albeit, with a different level of interfacial adhesion energy strength. First, infinite bead spacing would only ever lead to a creation of ridges for physical values of adhesion energy below the transition line (see Figure 3-3). This is readily seen in simulation by turning off bead-graphene interactions. Second, zero beads spacing (infinite number of beads) would mean the adhesion energy required to pass the transition from ridges to buckling would be unattainable, and so, only ridges would ever be observed as a result of the deformation. However, due to the high interfacial adhesion energy imposed in the scenario of infinite beads, the ridge does not stay upright after forming. A Lennard-Jones 12:6 wall is used for this infinite bead case to perform the simulations and the results match the no beads case in that the graphene only exhibits ridge formation and no buckling, as expected.

A power law relation exists between the adhesion energy at the transition point and the bead spacing of the substrate (see Figure 3-3) directly linking the different bead spacing values to different values of interfacial adhesion energy. The two parameters, spacing and adhesion energy, can be decoupled by relating each of them to configuration energy (see Figure 3-6). Configuration energy as made reference to in this thesis is the potential energy of a particular graphene sheet due to its geometry and deformation only, not including contributions from interfacial adhesion energy directly. The more tightly bound the graphene is to substrate the more strain energy is stored as graphene is deformed, resulting in a linear relation between configuration energy and interfacial adhesion energy (see Figure 3-6(a)).

The total configuration energy for transition from buckling to creating ridges relates to the distance between nanowires in the substrate through two channels: the number of buckled regions (n) and the deformation energy (U_b) of each buckled

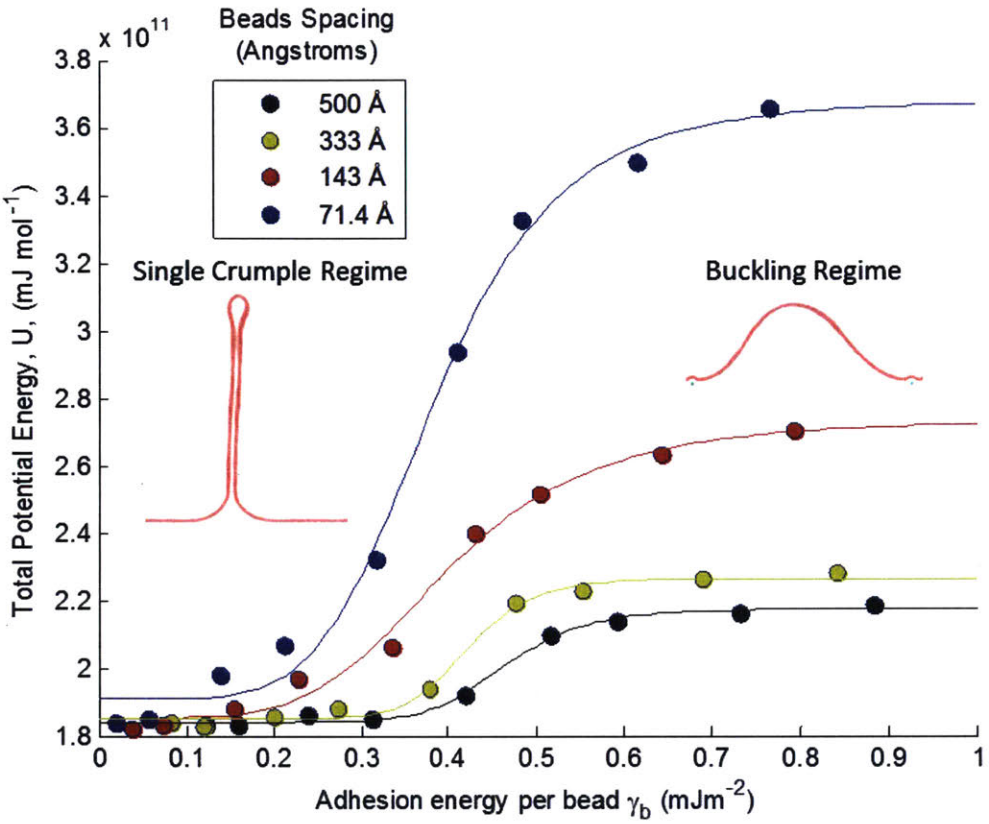

Figure 3-5: **Normalized configuration energy of the compressed graphene on top of substrates with different bead spacing.** As the nanowire spacing decreases the energy required to deviate from the single ridge regime increases, especially for high interfacial adhesion energy systems. For these systems ridge formation becomes a less energetically favorable deformation mechanism in favor of the more easily accessible buckling on top of more packed beads. The adhesion energy is normalized to one bead in order to account for the unequal number of identical beads in simulations with different nanowire spacing. This also shows that the transition point happens at around the same adhesion energy per bead. Hill equations [1,2] were used to fit the data and find the transition energies for each beads spacing. The equations are of the form $U = g\left[\left(\frac{c}{\gamma_b}\right)^{n+1}\right]^{-1} + s$, where U and γ_b are the total potential energy and adhesion energy per bead, respectively, and g, c, n, and s are fitting parameters of the Hill equations. The transition energies per bead are clustered around 0.40 mJm^{-2} per bead at 0.46, 0.42, 0.37, and 0.36 mJm^{-2} per bead for beads spacing of 500, 333, 143, and 71.4 Å, respectively.

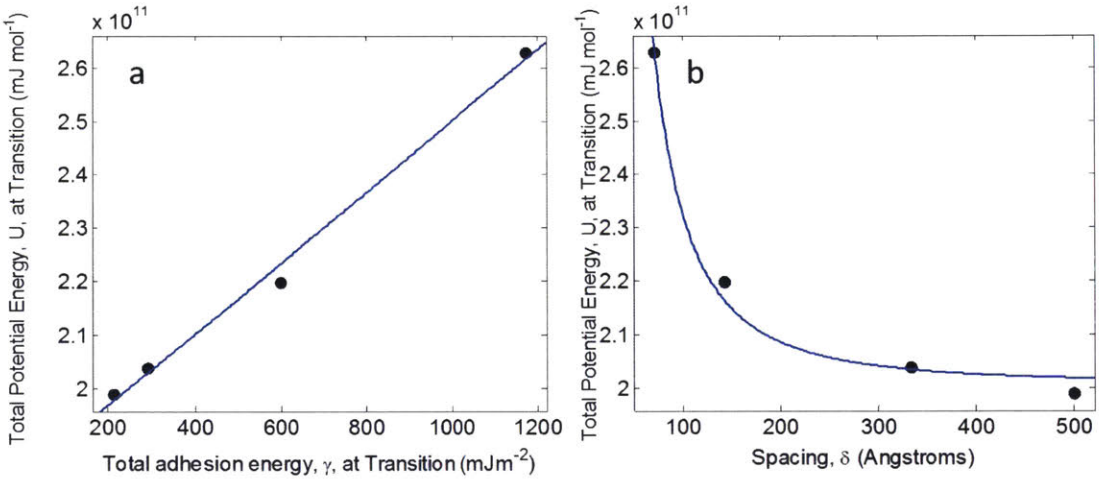

Figure 3-6: **Different relationships between the total configuration potential energy of deformed graphene sheets viewed through different lenses.** (a) The potential energy as a function of the adhesion energy is linear $U = \left[6.636 \times 10^{7}\left(\mathrm{m^2\,mol^{-1}}\right)\right]\gamma + \left[1.837 \times 10^{11}\left(\mathrm{mJ\,mol^{-1}}\right)\right]$, (b) as a function of the spacing the relationship takes the form of an inverse square law $U = \left[3.209 \times 10^{14}\left(\mathrm{mJ\ \AA^2\ mol^{-1}}\right)\right]\delta^{-2} + \left[2.007 \times 10^{11}\left(\mathrm{mJ\,mol^{-1}}\right)\right]$ by referring to Eq. (3.3). This is expected as there was shown to be a power law relationship between total adhesion energy and spacing providing a design criterion for graphene nanodevices. It is readily seen that control of interfacial adhesion energy is more favorable as it exhibits a linear response with respect to graphene configuration.

region. From plate theory, the general form of the bending energy of each buckled region is given in equation 3.1,

$$U_b = \int_S \frac{1}{2} EI\kappa^2 \, dS \tag{3.1}$$

where EI is the bending stiffness, κ is the local curvature of the plate, and S is the surface of integration that equals to δb (b is the width constant of the graphene in the direction normal to the loading) for the current setup of compression in one direction. Curvature is expressed as the reciprocal of the radius of curvature, which, as shown in Figure 3-4, can be assumed to be proportional to δ in the substrate with a factor of a_0, as shown in equation 3.2,

$$\kappa = \frac{a_0}{\delta} \tag{3.2}$$

One more step is required to account for the length of a graphene sheet (L) that yields the number of buckled regions as $n = L/\delta$, and summing up the bending energy of each buckled region to arrive at the form of equation 3.3,

$$U = nU_b + U_0 = \left(\frac{L}{\delta}\right) \frac{1}{2} EI \left[\frac{a_0}{\delta}\right]^2 \delta b + U_0 = \frac{a^2}{\delta} + c \tag{3.3}$$

where U is the total configuration energy, δ is the nanowire spacing in the substrate, $a = \frac{1}{2} bLEIa_0^2$ is a proportionality constant that relates to the bending stiffness (EI) and the total surface area of graphene (bL) and $c = U_0$ is a constant that accounts for the potential energy of the atomistic system without deformation. In accordance with this analysis an inverse square law is fit to the data (see Figure 3-6(b)), and find good agreement recovering the power law relation, this time from mechanics consideration. Knowledge of these relations is useful for the design of graphene topologies on substrate and for deciding which parameter to control depending on the desired shape of a graphene system. Moreover, since there was shown to be a power law relationship between total adhesion energy and spacing at the transition between graphene folding and stacking (Figure 3-3) these relations provide a design criterion

for graphene nanodevices. Wherein the two parameters are no longer independent, choice of substrate set the adhesion energy at the interface thereby dictating spacing between graphene ridges. Interfacial adhesion energy can be controlled by the choice of substrate. Bead spacing can similarly be controlled by choice of substrate and can also be tailored [113]. The next chapter will explore this idea of controlling graphene topology further.

Chapter 4

Graphene ridge formation mechanism during substrate-mediated compression

4.1 Introduction

The second part of this thesis aims at advancing the fundamental understanding of the intrinsic mechanisms that underlie the substrate-induced deformation of graphene by providing a theoretical description of such processes. More specifically, the focus is shifted onto the delamination process, which is a crucial initial step, and the subsequent ridge formation. Chapter 3 was concerned with surveying the different geometries that are possible with substrate-mediated compression and identifying and analyzing two parameters of the graphene-substrate interface. It was shown in Chapter 3 that there is a relationship between adhesion energy and spacing of heterogeneities on the substrate surface that is directly linked to graphene forming ridges or merely buckling before ridges could form. Moreover, good agreement from simple plate theory and data was shown to be able to account for the transition between the two states of ridges forming or not provided the potential energy of the system could be quantified, which it could be in simulation. Equipped with this knowledge,

Chapter 4 proceeds to analyze the more interesting of the two deformation regimes outlined in the previous chapter, ridges.

Fracture mechanics theory and molecular dynamics (MD) simulations are evoked to study the early deformation stages: right after delamination and up to the self-adhesion of graphene on the substrate. This allows to gain insights into the atomistic mechanisms underlying the formation, evolution, and localization of graphene ridges. While experimental findings are limited to macroscopic features, excluding any atomic level events associated with graphene buckling and the subsequent stacking of the out-of-plane sections, MD simulations reveal the atomic-scale mechanisms of graphene deformation on substrate under compressive loading, which control the morphology of graphene and the density of three-dimensional surface features. These simulations enable observation of graphene's intrinsic tendency to self-adhere, or stack, after buckling and upon further compression. This fundamental understanding could pave the way for more rational and controlled strategies, not only for developing three-dimensional graphene-based nano-architectures, but also many other strain engineering applications of two-dimensional materials.

4.2 Methods

4.2.1 Model setup and simulation details

The model setup consists of an initially flat graphene nanoribbon (monolayer) resting atop a deliberately undefined bulk-like substrate, whose interacting properties are controlled in simulation. The substrate is kept undefined to maintain generality and focus on certain features of the graphene-substrate interface, with no interference from specificities of different substrates. The dimensions of the system are 100 nm by 10 nm for the finite graphene nanoribbon as shown in Figure 4-1. Since the bulk substrate has no roughness as is, and has no modular elements, asperities are introduced to compensate for this fact, modeled as particles with a 1 nm van der Waals radius, on the substrate to account for possible surface heterogeneity. Keeping

to the same scheme employed in Chapter 3, a rigid substrate model is used with seven rows of nanowires to model the asperities (see Figure 4-1). The substrate with asperities can be used to describe heterogeneity through three different channels: The first option is modulating spacing between the nanowires to vary the topology of the substrate surface (14.3 nm in Fig. 4-1). Second, changing the discrepancy of the equilibrium separation distance between the graphene and the substrate at the asperities (see Figure 4-1a, side view). Third, varying the adhesion energy at the asperities to differentiate from that of the rest of the substrate. Among all these sources of heterogeneities to simulate roughness, the last one is chosen as the control parameter, since it most closely relates to the delamination process at the interface. It is then varied to effectively create different substrates and interfaces with different interfacial adhesion energies. In the initial setup for this heterogeneous system, the vertical (z-direction) equilibrium separation distance between the bulk substrate and graphene is 3.35 ÃĚ; the vertical equilibrium separation between the graphene and the substrate asperities is 3.76 Å (this creates a 0.21 Å step at the asperities).

For comparison, in addition to this heterogeneous substrate with asperities, a homogeneous substrate is also studied as a model of a perfectly smooth counterpart (see Fig. 4-1b). This homogeneous substrate has no intrinsic heterogeneities, so there are no disparities of adhesion energy at the interface with graphene. In such a system, when varying the adhesion energy to generate different homogeneous substrates, this change applies to the whole interface homogeneously, as opposed to the localized change happening in the heterogeneous substrate. Furthermore, to compare the behavior of graphene and its deformation in both types of substrate, heterogeneous and homogeneous, an effective interfacial adhesion energy (γ_0) is defined. The goal of the effective interfacial adhesion energy is to concisely provide a single parameter to compare the two types of substrate. For the heterogeneous substrate this effective adhesion energy is a function of the adhesion energy from the asperities and the bulk substrate. In practice, when performing simulations only the adhesion energy of the asperities is taken as a parameter, while the adhesion energy of bulk substrate is constant. Thus, in the heterogeneous substrate, the changes in the effective adhesion

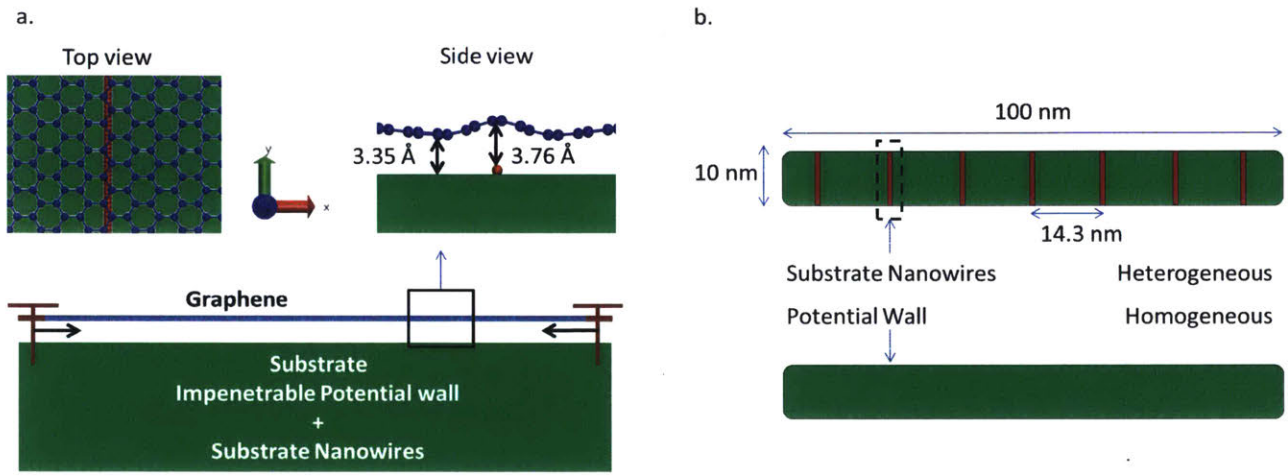

Figure 4-1: **Model Setup.** (a.) Graphene nanoribbon is modeled on a substrate with set surface features. Fully atomistic graphene (shown in blue) and Lennard-Jones components modeling the substrate are used in the molecular dynamics simulations. The graphene nanoribbon and substrate are compressed under displacement boundary conditions. The edges of the graphene nanoribbon (shown in brown) are clamped and compression is done in the armchair direction. For a heterogeneous substrate, asperities can be considered as nanowires (as in Chapter 3, shown in red) are introduced on the bulk-like substrate (shown in green). The asperities resemble surface features of physical substrates, such as roughness, composite substrates that are overlaid with nanowires, or substrates with tailored surface features. (b.) The homogeneous substrate is made of a 9:3 type Lennard-Jones potential wall whose energy well is varied to change the interfacial adhesion energy. The heterogeneous substrate is made up of both a 9:3 type Lennard-Jones potential wall whose energy well is kept constant and 12:6 Lennard-Jones particles arranged in rows whose energy wells are varied to change the effective interfacial adhesion energy.

energy are only coming from the adhesion energy of the asperities. For the homogeneous substrate, the effective adhesion energy is simply the adhesion energy of the bulk substrate, which is indeed the parameter evoked in the simulations.

For the MD simulations, the atomistic behavior of the graphene nanoribbon is modeled with the same Morse-based potential used in Chapter 3. The functional forms and parameters for all the potentials used are summarized in Table A.1. Understandably, an unreactive potential formulation is not able to capture bond-breaking/forming features, but such mechanisms are beyond the scope of the present work. The bulk substrate is modeled as a computationally impenetrable wall that behaves as a bed of nonlinear springs interacting with the graphene as a function of perpendicular distance to the wall as a Lennard-Jones potential wall [19,98,114]. The asperities on the substrate, when considered, will interact with the graphene through a Lennard-Jones potential (Table A.1). The model setup follows from that developed in Chapter 3. Chapter 4 however, restricts the attention to two different substrates: a homogeneous substrate and a heterogeneous substrate. This is because while Chapter 3 aimed at understanding what were the key parameters of substrate-mediated compression of graphene and how they affected the final deformed graphene, Chapter 4 is more focused on the atomistic mechanisms giving rise to ridge formation and the effect of spatial distribution of adhesion energy at the interface on such a process.

4.2.2 Implementation of mechanical constraints

Displacement controlled boundary conditions are imposed on the graphene nanoribbon as in Chapter 3 keeping left and right edges of the nanoribbon clamped while the top and bottom edges are simply supported. The potential wall is effectively infinite in the simulations as it covers the entire simulation box below the graphene. Such an implementation creates no strain mismatch with the graphene lattice since any carbon atoms found within the potential cutoff radius of the wall will have the same interaction with the wall. Asperities placed on this potential wall, however, do allow for a strain mismatch with the substrate during compression, as they break the homogeneity of the potential wall. Asperities, thus, cause graphene to slide over the

substrate during compression with varying difficulty as the adhesion strength between graphene and asperities is changed.

The short edges of the graphene nanoribbon are clamped (see bottom part of Fig. 4-1a), while the entire simulation box is compressed in the lateral (x-direction) at a constant strain rate of 0.2/ns. Such a high strain rate is necessary in MD simulations for keeping time scales tractable, since real strain rates are computationally unaffordable for simulation. Lower strain rates (0.02 and 0.002/ns) were also used to check for strain rate effects, but no appreciable difference in the simulations resulted in terms of critical energy release rate ($< 3\%$ at 300 K), deformation shape or observed mechanisms.

4.2.3 Fracture mechanics analysis

The delamination process, which is the first necessary step for the generation of three-dimensional surface features, is inherently one of separation and creation of surfaces. Thus, a fracture mechanics approach is taken to provide a theoretical framework for this observed phenomena. Unlike previous studies [114] that considered breaking of actual graphene covalent bonds in the presence of pre-cracks, here the focus is on the fracture process at the perfectly bonded biomaterial interface between graphene and substrate, namely the delamination process. Accordingly, the analysis proceeds with calculating the energy release rate and critical energy release rate for the deformation and delamination processes of the graphene-substrate interface, respectively, within the context of fracture mechanics theory. This energy release rate is expressed as the work done on the system in order to change the area of the intact interface, which is described in equation 4.1 [115,116],

$$G = \frac{1}{\Delta A} \int F_x \, dx \tag{4.1}$$

where $\Delta A = bx_0$ is the area of the delaminated section of the interface, b is the width of the graphene nanoribbon, x_0 is the final length of the delaminated section, x is the displacement, and F_x is the force on the simulation box. The critical energy release

rate can be considered with two parts as [117]

$$G_c = \gamma_0 + \gamma_{\text{diss}} \tag{4.2}$$

where γ_0 is the graphene-substrate surface energy and γ_{diss} is the dissipative energy term associated with delamination processes at the interface.

4.3 Results and discussion

4.3.1 Atomistic mechanisms of deformation

Molecular dynamics simulations complemented by the fracture mechanics analysis mentioned above, a step-by-step description of the deformation mechanism of graphene is elaborated. The deformation happens at the nanoscale as graphene is subjected to axial compression forces. Figure 4-2 shows the energy release rate calculated throughout the whole deformation process. As graphene is compressed, it stores elastic energy up to the so-called critical point, in which the increment in elastic energy is enough to overcome the energy required to create surfaces at the interface (γ_0), and to dissipate the extra energy during delamination (γ_{diss}). This behavior defers from brittle materials that undergo so-called mode I crack extension, i.e. the critical point is reached as soon as the energy required to create surfaces is reached. Instead, the graphene-substrate interface possesses an extra dissipative energy contribution to its energy release rate at the critical point that scales with the interfacial adhesion energy. Thus, the dissipative energy contribution arises as a consequence of: (1) the incongruence between the load and the displacement of the delamination. Accordingly, not all the work done by the lateral force gets converted into useful work for creating new surfaces at the interface, but rather partially dissipated. Furthermore, additional extra energy is also required (2) to initiate the delamination at a perfectly adhered interface. This is opposed to the propagation mechanism on a perfect interface, like the one considered in simulations for the homogeneous substrates.

For the graphene-substrate interface the critical energy release rate is reached at

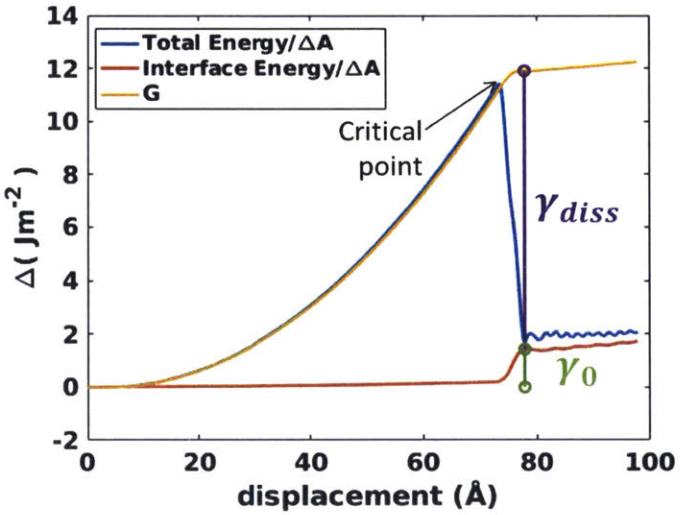

Figure 4-2: **Components of critical energy release rate.** The energy release rate is calculated throughout the whole deformation process up to the critical point. The energy release rate closely follows the potential energy of the system until it becomes greater than the potential energy of the system at which point the critical energy release rate is reached and plateaus. The potential energy drops as the stored energy in the graphene nanoribbon is released. The change in interfacial energy is also plotted showing no net change as the graphene and substrate are perfectly laminated in the beginning of the deformation, but as soon as delamination happens the change in interfacial adhesion energy normalized by the delamination area exactly equals the effective interfacial adhesion energy prescribed in the simulation, as expected.

the critical point and marks the initiation of the delamination process, right when the graphene nanoribbon loses its ability to carry any more lateral load and starts it separation from the substrate. The case of the substrate provides a better illustration the components of this critical energy release rate for delamination. Figure 4-2 shows a representative energy release rate plot as a function of lateral displacement during compression. As the graphene is compressed more elastic energy is stored and therefore the energy release rate increases up to the critical point of delamination, where the elastic energy is then released and the lateral load carrying capacity drops accordingly. When this happens, the energy release rate plateaus at its critical value, where the graphene delaminates. The critical energy release rate is a material property of graphene-substrate interface. Figure 4-2 also plots the change in effective interfacial adhesion energy, recovering the value prescribed (1.424 Jm^{-2}) in simulation.

The details of the actual deformation mechanisms of graphene ridge formation are described based on fully atomistic simulations. Figure 4-3 shows the details of ridge formation process, where the bottom panel depicts all the steps A to F. After compression, graphene first buckles out of plane (Figure 4-3A). This buckling is follow by a collapse of the sinusoidal shape of graphene, with a rapid increase of the delamination area. It can be seen as if the graphene sheet is being torn off the substrate from the initial delamination, evidenced by its rapid and large separation from the substrate. This is quickly remedied as compression goes on by a sort of self-healing process by which the edges of the delaminated area reattach to the substrate (Figure 4-3B), and the base of the ridge gets *pinched-in* (Figure 4-3C). Whether this self-healing mechanism is a physical phenomenon for single layer graphene on a substrate is not completely clear, but according to the simulation results presented this is a plausible mechanism that allows for graphene resuming compression. Furthermore, this may be a hypothetical mechanism to explain how ridges are able to form later on in the process, which implies the need of delaminated material for such ridge formation. Pinching in at the base of the ridge (Figure 4-3D) sets the stage for self-adhesion (Figure 4-3E) as compression continues. This *pinching-in* effect, which implies self-adhesion, or stacking, is facilitated by van der Waals forces between different sections

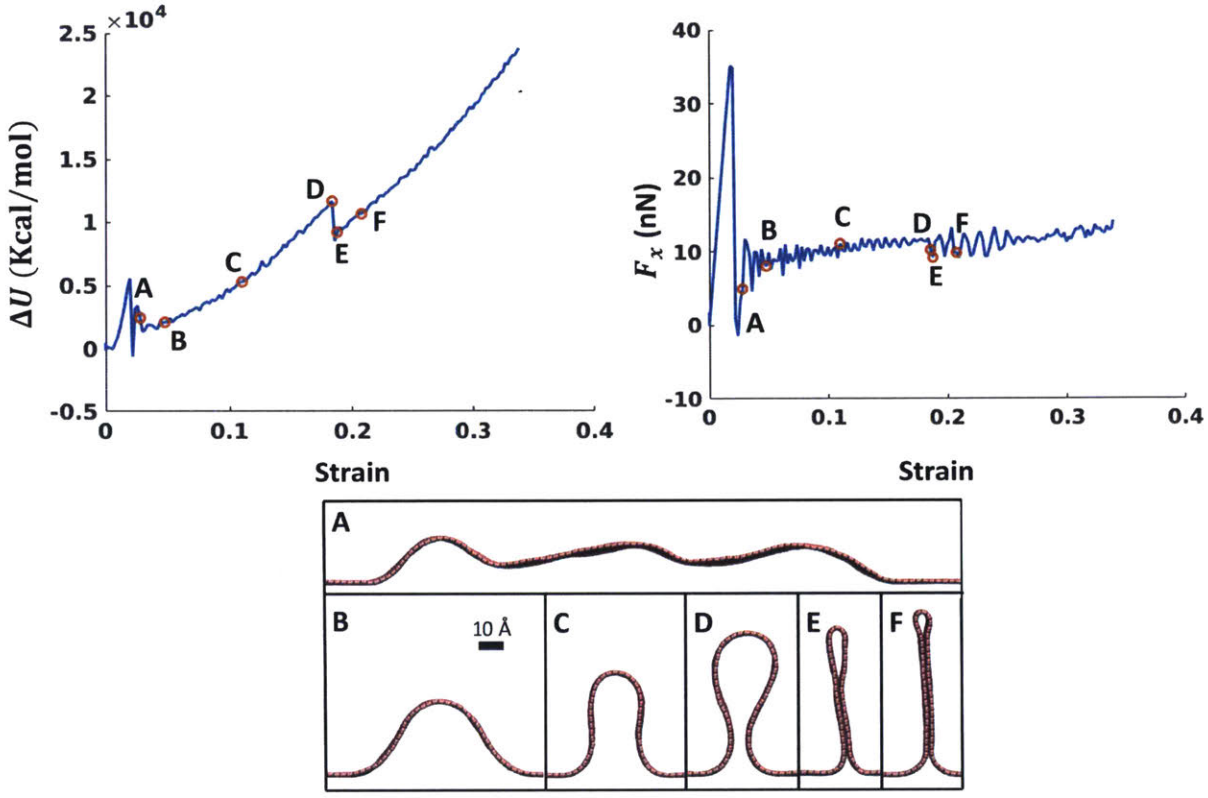

Figure 4-3: **Atomistic ridge formation mechanism.** Graphene is compressed up to a critical force after which delaminated buckling occurs followed by a transient tearing off of the substrate (A) that leaves behind a large delaminated area. As compression continues the edges of the delaminated area re-adhere (B) and the graphene film starts to grow out of plane (C). In part due to the original large delaminated area at buckling, there is some free-standing graphene held up above the substrate-supported graphene which does not get compressed by the substrate creating a pinching effect (D) at the base of the delaminated region of graphene. Further compression guarantees self-adhesion (E) of the graphene creating a ridge after this pinching in effect and grows the ridge taller (F). Self-adhesion (D $\rightarrow$ E) is energetically favorable because it decreases the area of free surface caused by delamination and less graphene is subject to bending. Load displacement curves show a linear increase in load as the graphene-substrate composite is compressed up to the point of initial delamination. This point corresponds to the attainment of the critical energy release rate at the interface, delamination initiation, dissipation of stored strain energy (A) in the graphene nanoribbon, and the onset of delaminated buckling.

of the graphene nanoribbon, and might also be due to transient $\pi - \pi$ stacking that occurs as the ridge grows out of plane after the graphene self-adheres. Once the neighboring carbon atoms that have delaminated from the substrate come close enough, as the rest of the graphene nanoribbon slides inwards during compression, they will stack and form the folded out-of-plane ridge. Furthermore, this *pinching-in* phenomenon could not have been possible without the previous uncontrolled popping off of graphene section that followed the initial delamination, as shown in Figure 4-3A. Indeed, this phase of temporary increased delamination area (Figure 4-3A) that follows the initial delamination is also characterized by mobility of the delaminated graphene sections. This movement quickly stops when the tips of the delamination re-adhere to the substrate (Figure 4-3B), thus, anchoring the delaminated portions of the graphene nanoribbon. The *pinching-in* occurs during this quiescence of the now free-standing delaminated regions of graphene (Figure 4-3C). After delamination the lateral (x-component of) stress in the graphene is diminished allowing the tips of the delaminated region to re-adhere to the substrate (Figure 4-3A, B). The bonded sections of the graphene are compressed further in than the delaminated graphene regions creating the *pinching-in* effect (Figure 4-3D). It becomes inevitable for the two inside faces of the delaminated graphene to adhere, completing the ridge formation as compression continues (Figure 4-3F).

4.3.2 Graphene-substrate interface properties

Simulations clearly show that weaker regions of adhesion in a heterogeneous substrate lead to self-adhering folding of the graphene nanoribbon and therefore to the formation of ridges after delaminated buckling. The simulations also show that stronger adhesion regions along the substrate suppress such delamination and therefore the subsequent ridge formation for the same level of strain. This behavior is in contrast with the mechanism observed for graphene over a homogeneous substrate, where there are no weak or strong regions of adhesion and the adhesion strength is uniform throughout the interface. In this case, no matter the level of adhesion energy, graphene will always yield self-adhering folds. Unlike the heterogeneous substrate,

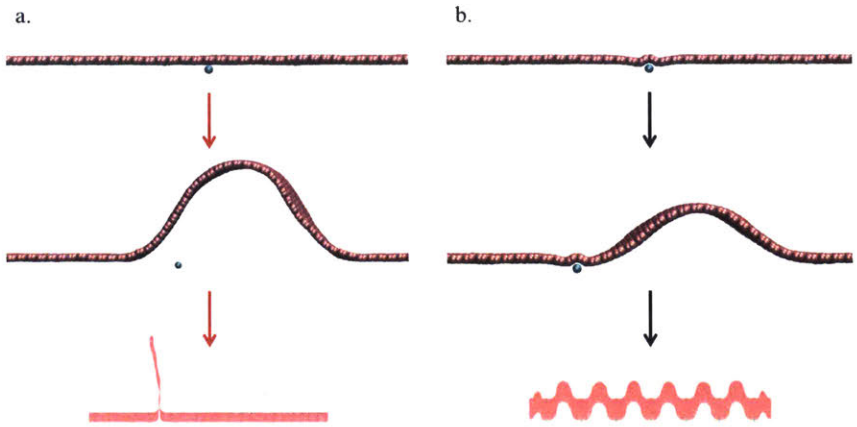

Figure 4-4: **Pinning at asperities.** Ridge formation depends on the ability of graphene to buckle out of plane and slide over the substrate. When asperities are on the substrate they become possible pinning locations of graphene inhibiting sliding. The asperities used in this chapter were modeled off the asperities used in Chapter 3, which provides further detail on the modeling choices and rationale. The strength of this interaction at the asperities determines the eventual shape of the graphene nanoribbon. A weaker interaction (a. 0.063 Jm^{-2}) will result in ridge formation. A more constraining interaction (b. 1.171 Jm^{-2}) will leave the graphene sheet unable to slide and pool in one location prohibiting in pinching in from happening and leaving the graphene stuck at a buckled shape without self-adhesion.

there will be no localized constraints hampering the graphene film from pinching in and forming ridges after delamination.

As the adhesion energy at the substrate asperities increases, graphene loses its ability to slide over the substrate and subsequently its ability to pinch in and self-adhere. This is most readily explained by the sticking of the graphene nanoribbon that happens at the region of high adhesion energy (Figure 4-4). The adhesion energy at the asperities (varying from 0.002 to 1.171 Jm^{-2}) is higher than this at the smooth sections of the substrate (constant 0.06 Jm^{-2}) (Figure 4-5). This creates a different response in terms of the critical energy release rate of the interface for heterogeneous and homogeneous substrates. For the heterogeneous substrate, the critical energy release rate plateaus and slightly diminishes beyond an adhesion energy of 0.588 Jm^{-2} (for comparison, interlayer graphene-graphene surface energy [17] is 0.260 Jm^{-2}). The critical energy release rate, and therefore, resistance to delamination, increases with

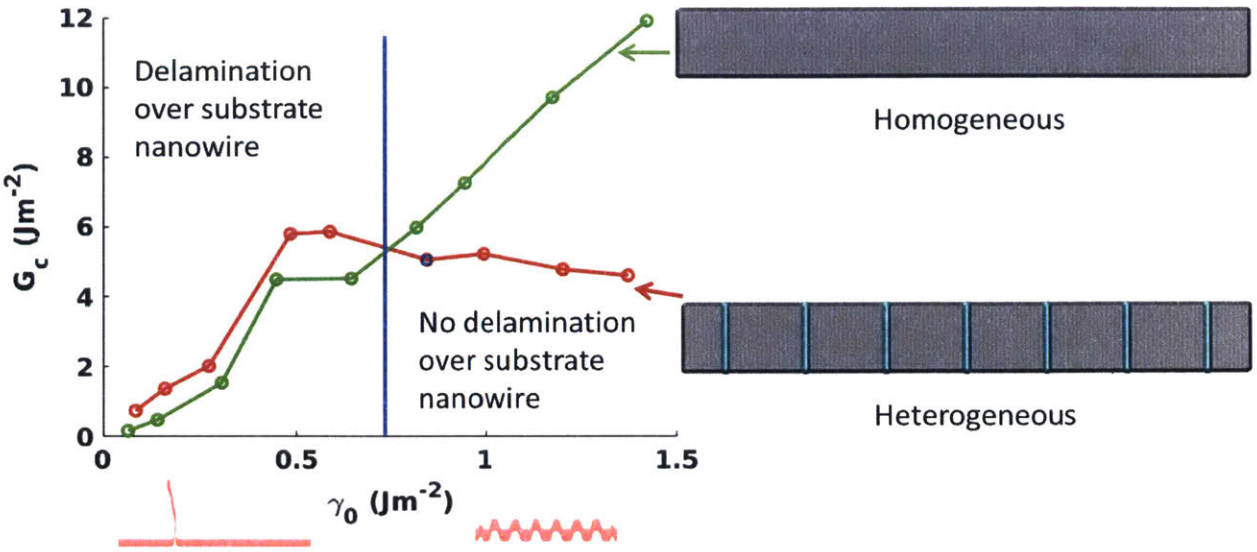

Figure 4-5: **Homogeneous versus heterogeneous substrate effects on interfacial energy release rate.** Critical energy release rates for two sets of substrates as a function of their effective interfacial adhesion energy shows why a transition from ridge formation to buckling without self-adhesion is seen in simulation. For the homogeneous substrate as the effective interfacial adhesion energy increases so does the critical energy release rate. However, the same does not apply for the heterogeneous substrate. Instead, the critical energy release rate of the heterogeneous substrates reaches a maximum as the adhesion energy at the asperities reaches a critical value that corresponds to a decrease in toughening ability. The high level of adhesion at the asperities creates an unfavorable stress intensification that weakens the interface leading to large areas of delamination between the asperities, which are in this case regions of localized high adhesion energy.

effective interfacial adhesion energy up to this point (0.588 Jm^{-2}) where critical energy release rates of the homogeneous and heterogeneous substrates intersect in Figure 4-5.

Higher adhesion energy at the asperities compared to the rest of the substrate creates a source of stress intensification at the interface. The stress intensification at the asperities leads to lessening of the critical energy release rate [118]. This stress intensification is also partly due to the sharpness of the high adhesion region, here being the 10 Å van der Waals radii of the substrate asperities. There is no smooth transition of adhesion energy over a long distance, but instead a sharp transition that weakens the interface, as opposed to a smoother gradient that would be less disruptive and allow for the stress concentration to be more spread out. The homogeneous

substrate, on the other hand, exhibits increasing critical energy release rate as the adhesion energy increases across the whole interface (varies from 0.064 to 1.424 Jm^{-2}). The heterogeneity of the substrate breeds analogous heterogeneity in the adhesion energy at the interface and thus equally analogous heterogeneity in the proclivity for delamination across the interface. This heterogeneity can then be used to shape the delaminated structures *a priori*. In other words, the different delamination behavior of graphene regions depending on the adhesion strength to the substrate, opens the door to a rational design of out-of-plane structures of graphene. Controlling the composition and heterogeneity of the substrate controls the adhesion energy, which in turn controls the delamination process and therefore the formation of ridges.

4.3.3 Substrate design

The heterogeneous substrate with asperities models a composite substrate with nanowires embedded on a potential wall. Simulations with the heterogeneous substrate show how a sharp localized gradient in adhesion energy can influence graphene topology under compression. Given this observation about adhesion energy difference, a composite substrate is generated by introducing 33.3 nm-wide ($\frac{L_0}{3}$) alternating regions of relatively weak (0.140 Jm^{-2}) and strong (0.447 Jm^{-2}) adhesion energy in the graphene-substrate interface to demonstrate the possibility of rational control over the location of ridges in graphene (Figure 4-6). As predicted, regions of weak adhesion more readily buckle out of plane, and self-adhere into ridges upon further compression. This can lead to a more direct level of control of three-dimensional geometries by using tailored substrates with adhesion-energy patterned regions, where the relative energy difference between regions plays a key role.

Another aspect to consider when controlling the formation of three-dimensional structures is the density of graphene ridges in addition to their location. Controlling the spatial density is done by introducing a gradient in the values of the adhesion energy along the substrate, but controlling simultaneously the number of ridges in a specific region of the graphene nanoribbon, which requires stricter constraints on the graphene-substrate interface. When a ridge forms in the graphene, its out-of-plane

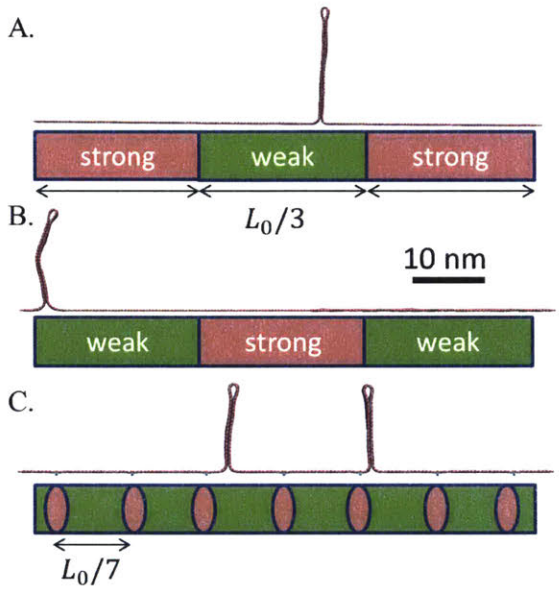

Figure 4-6: **Ridge location and spacing can be tuned via substrate design.** Using strong (0.447 Jm^{-2}) and weak (0.140 Jm^{-2}) regions of adhesion allows control of ridge nucleation location (A). The difference in strong and weak adhesion regions can be within 10% and the effect would still be enough control where ridges form. On a large scale, adhesion energy patterning can be used to tune frequency of graphene ridges. The effect of ridge-ridge annihilation is clearly seen when creating two weak regions of adhesion and observing only one ridge forming (B). Control on ridge number is not as easily achieved through adhesion alone (C; strong: 1.177, weak: 0.447 Jm^{-2}) even with introduction of asperities.

growth is fed by the surrounding planar regions of the graphene, suppressing wrinkles and buckling in this planar regions and preventing other ridges to form. Therefore, increasing the total number of ridges that form in graphene sheet of the same size requires eliminating such ridge-ridge annihilation. A possible way to circumvent these ridge-ridge interactions is increasing the length of graphene, so more planar graphene is available to feed additional ridges, or to partition the graphene nanoribbon in such a way that ridges are not able to interact. The latter holds the advantage of not needing more graphene to achieve the same goal. Additionally, partitioning, or compartmentalizing single ridge areas, of the graphene nanoribbon also controls the height of the ridges, which is important for fine-tuning of the three-dimensional structure of graphene. Actually, ridge height will necessarily be different for the same graphene sheet when it has different number of ridges protruding from it. Assuming equal size of coexisting ridges their height can be calculated as,

$$h_R = \frac{\varepsilon_{sa} L_0}{2N} \tag{4.3}$$

where h_R is the individual ridge height, ε_{sa} is the level of strain after self-adhesion has already occurred, L_0 is the original length of the flat graphene in the direction parallel to compression, and N is the number of ridges. The factor of 2 accounts for each ridge having two faces that need to meet to form a ridge. For instance, for a homogeneous substrate that is pinned to the graphene across its width (perpendicular to direction of compression) at seven equally spaced points, seven ridges of approximately equal height are formed (Figure 4-7). Pinning the graphene to the substrate is one way to achieve control of ridge number. Partitioning can also be achieved although less predictably without pinning through controlling the length scales of the adhesion gradients. Partitioning in this sense means to ensure there is enough of a barrier between separate sections of graphene prohibiting ridge-ridge interactions to occur. Partitioned ridges would not be able to annihilate one another and this can lead to creation of more ridges compared to the baseline case without partitioning. Thus, partitioning controls ridge number and adhesion energy gradients control location

Figure 4-7: **Partitioning can control ridge number and height.** Pinning graphene to the substrate to eliminate sliding of graphene over substrate enables control of ridge number. Eliminating sliding effectively eliminates ridge-ridge annihilation and allows ridges to form on opposite sides of the pinned graphene.

so that the two control density and wavelength of ridge formation. The challenges then become clear to partition a graphene sheet into sections and to manipulate the adhesion energy profile of the interface.

THIS PAGE INTENTIONALLY LEFT BLANK

Chapter 5

Summary and outlook

This thesis has focused on graphene deformation that extends further out of plane than wrinkling [119]. Nonlinearities of the graphene sheet complicate the problem beyond a simple analytical model. The work presented in Chapter 3 is motivated by a need for finding a simple relation from the inherent properties of graphene and substrate that can be used to guide design of graphene in interfaces. This design guide will allow for masterful applications of complicated geometries in future graphene-based devices. The existing body of work on graphene merits and gives itself to a desire for understanding the mechanics of graphene to better design experiments, interfaces, and devices.

Chapter 3 emphasizes the difference between passive and actively achieved configurations of graphene to further distinguish between wrinkling and ridge formation of graphene on substrate. Although, both behaviors depend on the same parameters, substrate surface and interfacial adhesion energy, the shape of graphene is markedly different. Nonetheless, it is helpful to build on the existing work on wrinkling by making the analogy with graphene ridge formation. Where wrinkling exhibits a transition that is dependent on interfacial adhesion energy [57], so does the process of ridge formation. The transition for wrinkling is between graphene (1) fully conforming to the underlying substrate and (2) remaining flat over the substrate. Similarly, ridge formation exhibits a transition between (1) forming self-adhering extrusions (ridges) and (2) buckling with delamination (absence of ridges).

Ridge formation and wrinkling will both have a role in designing future graphene nanoelectronic mechanical systems. In the first part of this thesis it was shown that ridge formation can be fine-tuned by choice of substrate alone or choice of substrate and tailoring its surface. As more work is done on these processes more will be explored through simulation and experimentation relating to the key parameters that control other transition points between different configurations for graphene. The second part of this thesis presents a more analytical approach combined with simulation techniques to further elucidate the atomistic mechanisms that give rise to graphene ridge formation. Experiments that follow earlier work compressing graphene on different substrates, and simulations that probe more than just the interfacial adhesion energy and substrate surface topology are future directions in this field that will provide further insights.

Generating three-dimensional features in two-dimensional materials such as graphene is one of the most promising strategies to achieve new properties and more advanced applications. However, controlling the actual three-dimensional structures for the desired properties requires fundamental understating of the formation mechanisms of these three-dimensional entities. Using MD simulations, and within the context of fracture mechanics theory, this works aims to garner some of this fundamental understanding on the underlying mechanisms that control the formation of ridges of different shapes on graphene.

Chapter 4 shows the dependence of graphene out-of-plane shapes on substrate composition and heterogeneity. Consequently, it was shown how a proper selection and design of the substrate can yield tailored surface topologies of graphene thin films, with the potential of nanoscale precision, when these are deformed under compression on such substrate. More specifically, the contrast between ridge formations over heterogeneous or homogeneous substrate is highlighted. The design of substrate heterogeneities provides a departure from the reliance on graphene sheet size to control ridge spacing; ridge spacing can be varied without changing the size of the graphene sheet. Additionally, strain and ridge spacing allows for control of ridge height simply by conservation. For two graphene nanoribbons of the same size that are strained the

same amount, the one with higher spacing between ridges will have shorter ridges. The difference would then necessarily be the underlying substrate as demonstrated in this work.

Chapter 4 also shows that ridge formation in graphene is the result of a mismatched strain that arises between delaminated and adhered sections of graphene film during substrate-mediated compression. This mismatch within the graphene film leads to a *pinching-in* effect that facilitates self-adhesion, or stacking, of the concave side of delaminated buckles during compression. Such self-adhesion during ridge formation lowers the energy of graphene through two channels: 1) The bending energy of the graphene film is decreased by localizing the bending regions at the ridge. 2) Self-adhesion decreases the free surface of the graphene and stabilizes the system by stacking of two layers with van der Waals interaction. This can also be due to transient $\pi - \pi$ stacking that occurs as the ridge grows out of plane after the graphene self-adheres. However, as the ridge grows this $\pi - \pi$ stacking is constantly lost and regained as the walls of the ridge shift over each other during compression. The behavior of the ridge walls during compression can thus be an interesting avenue of research for nanoscale sensing technologies.

This thesis has focused on an in-depth study of the case of uniaxial compression, but further work can be done to exploit the potential of ridge spacing control with biaxial compression to create more elaborate three-dimensional shapes. This future direction is further justified by previous experimental work that has created ridge patterns with biaxial compression [19,32,36]. A similar study, as presented in thesis, to elucidate the atomistic mechanisms involved in biaxial compression would give more insight for design of graphene ridge patterns. Furthermore, only single layer graphene is presented in this work, which also leaves room for expansion to multilayer graphene. This work sets the basis for further studies on the topic. Results presented here from molecular dynamics simulations can be carried over to novel experimental research to reproduce these simulation findings and to benchmark efficiency gains from controlled topologies with existing deformed graphene devices. This work, and future studies, can spur experimental studies to propose possible schemes to control

ridge architectures via substrate engineering.

Appendix A

Tables

Table A.1: Functional forms and parameters of potentials used in simulations.

Carbon-Carbon interactions			
$E_{\text{Morse}} = D\left[1 - e^{-\alpha(r-r_0)}\right]^2$	$D = 114.460\,\text{kcal mol}^{-1}$	$\alpha = 2.1867\text{Å}^{-1}$	$r_0 = 1.418\text{Å}$
$E_{\text{dihedral}} = K\left[1 + d\cos\left(n\phi\right)\right]$	$K = 3.001\,\text{kcal mol}^{-1}$	$d = -1$	$n = 2$
$E_{12:6-LJ} = 4\epsilon\left[\left(\frac{\sigma}{r}\right)^{12} - \left(\frac{\sigma}{r}\right)^{6}\right]$	$\epsilon = 0.0861\,\text{kcal mol}^{-1}$	$\sigma = 3.4\text{Å}$	
$E_{cos-squared} = K\left[\cos\theta - \cos\theta_0\right]^2$	$K = 67.185\,\text{kcal mol}^{-1}$	$\theta_0 = 120°$	
Carbon-bead interaction			
$E_{12:6-LJ} = 4\epsilon\left[\left(\frac{\sigma}{r}\right)^{12} - \left(\frac{\sigma}{r}\right)^{6}\right]$	ϵ varies	$\sigma = 3.35\text{Å}$	
Carbon-wall interaction			
$E_{9:3-LJ} = \epsilon\left[\frac{2}{15}\left(\frac{\sigma}{r}\right)^{9} - \left(\frac{\sigma}{r}\right)^{3}\right]$	ϵ varies	$\sigma = 3.35\sqrt[6]{\frac{5}{2}}\text{Å}$	

Table A.2: Value of interfacial adhesion energy as a function of bead spacing and the Lennard-Jones (LJ) energy parameter used in the simulation. Using the same set of LJ energy parameters yields different interfacial adhesion energies due to the increased numbers of beads (nanowires) on the substrate for lower spacing.

Lennard-Jones energy parameter [kcal mol^{-1}]	Spacing (Å)			
	500	333	143	71.4
	Interfacial Adhesion Energy [mJm^{-2}]			
0.03577	56.7	57.6	61.2	67.5
0.35767	73.4	82.6	119.8	184.5
1.03723	111.4	139.6	251.7	448.3
1.60950	145.8	191.2	371.3	686.1
2.39637	195.5	265.7	545.9	1031.5
3.07594	241.3	334.2	705.2	1343.0
3.57667	276.4	386.6	826.7	1579.2
4.47084	340.5	482.5	1049.2	2013.9
5.43654	411.4	589.4	1295.3	2496.9

THIS PAGE INTENTIONALLY LEFT BLANK

Appendix B

Representative LAMMPS Script

```
processors * * 1
boundary p p p
units real
atom_ style molecular
timestep 2
dimension 3
read_ data data_ file.data
neighbor 5 bin
neigh_ modify every 1
bond_ style morse
bond_ coeff 1 114.460 2.1867 1.418
angle_ style cosine/squared
angle_ coeff 1 67.185 120.0
dihedral_ style harmonic
dihedral_ coeff 1 3.001 -1 2
pair_ style lj/cut 10
pair_ coeff * * 0.0861 3.4
region 99 block INF INF INF INF INF -2.90 units box
group wallsub region 99
region 1 block INF 5 INF INF -2.90 INF units box
```

```
group moving region 1
region 2 block 991 INF INF INF -2.90 INF units box
group fixed region 2
region 3 block INF INF 93.2 INF -2.90 INF units box
group top region 3
region 4 block INF INF INF 4.5 -2.90 INF units box
group bottom region 4
group graphene subtract all wallsub
dump realtime all dcd 5000 dump.dcd
compute x_ max graphene reduce max x
compute x_ min graphene reduce min x
compute y_ max graphene reduce max y
compute y_ min graphene reduce min y
compute z_ max graphene reduce max z
compute z_ min graphene reduce min z
compute s1 graphene stress/atom
compute pegrp graphene pe/atom
compute pepair graphene pe/atom pair
compute pebnd graphene pe/atom bond
compute peang graphene pe/atom angle
compute pedhd graphene pe/atom dihedral
compute pesum graphene reduce sum c_ pegrp
compute sum1 graphene reduce sum c_ s1[1] c_ s1[2] c_ s1[3] c_ s1[4] c_
s1[5] c_ s1[6]
fix wallhi126 graphene wall/lj126 zlo -3.35 0.037701432 2.984511 5.00 pbc
yes units box
fix wallhi graphene wall/lj93 zlo -3.35 0.357667188 3.90272672 5.00 pbc
yes units box
fix_ modify wallhi energy yes
fix_ modify wallhi126 energy yes
```

```
velocity graphene create 300.00 376847 rot yes
fix nosehoover graphene nvt temp 300.0 300.0 300.0
thermo_ style custom step pxx pyy pzz pxy pxz pyz c_ sum1[1] c_ sum1[2]
c_ sum1[3] c_ sum1[4] c_ sum1[5] c_ sum1[6] lx ly lz temp c_ pesum ke etotal
enthalpy evdwl ecoul epair ebond eangle edihed eimp emol elong etail f_
wallhi f_ wallhi126 pe c_ x_ max c_ x_ min c_ y_ max c_ y_ min c_ z_ max
c_ z_ min
thermo_ modify flush yes
thermo 100
fix 23 all balance 0 xy 20 1.1
velocity moving set 0.00 NULL 0.00 units box rot yes
fix 1767 moving setforce 0.00 NULL 0.00
velocity fixed set 0.00 NULL 0.00 units box rot yes
fix 17676 fixed setforce 0.00 NULL 0.00
velocity top set NULL 0.00 NULL units box rot yes
fix 176789 top setforce NULL 0.00 NULL
velocity bottom set NULL 0.00 NULL units box rot yes
fix 1767898 bottom setforce NULL 0.00 NULL
velocity wallsub set 0.00 0.00 0.00 units box rot yes
fix 29999 wallsub setforce 0.00 0.00 0.00
min_ style cg
min_ modify dmax 0.1
minimize 0.0 0.0 10000 10000
run 100000
fix compress all deform 10 x erate -2e-7 remap x
run 1000000
unfix compress
run 500000
```

THIS PAGE INTENTIONALLY LEFT BLANK

Bibliography

[1] J. N. Weiss. The Hill equation revisited: uses and misuses. *The FASEB Journal*, 11(11):835–841, 1997.

[2] Richard Barlow and Joanna F. Blake. Hill coefficients and the logistic equation. *Trends in Pharmacological Sciences*, 10(11):440–441, 1989.

[3] Talal Al-Mulla and Markus J. Buehler. Origami: Folding creases through bending. *Nature Materials*, 14(4):366–368, 2015.

[4] Seoung Ki Lee, Beom Joon Kim, Houk Jang, Sung Cheol Yoon, Changjin Lee, Byung Hee Hong, John A. Rogers, Jeong Ho Cho, and Jong Hyun Ahn. Stretchable graphene transistors with printed dielectrics and gate electrodes. *Nano Letters*, 11(11):4642–4646, 2011.

[5] Keun Soo Kim, Yue Zhao, Houk Jang, Sang Yoon Lee, Jong Min Kim, Kwang S. Kim, Jong-Hyun Ahn, Philip Kim, Jae-Young Choi, and Byung Hee Hong. Large-scale pattern growth of graphene films for stretchable transparent electrodes. *Nature*, 457(7230):706–710, 2009.

[6] Weixia Zhang, Sudarat Lee, Kelly L. McNear, Ting Fung Chung, Seunghyun Lee, Kyunghoon Lee, Scott A. Crist, Timothy L. Ratliff, Zhaohui Zhong, Yong P. Chen, and Chen Yang. Use of graphene as protection film in biological environments. *Scientific Reports*, 4:4097, 2014.

[7] Jingquan Liu, Liang Cui, and Dusan Losic. Graphene and graphene oxide as new nanocarriers for drug delivery applications. *Acta Biomaterialia*, 9(12):9243–9257, 2013.

[8] Yan Wang, Li Wang, Tingting Yang, Xiao Li, Xiaobei Zang, Miao Zhu, Kunlin Wang, Dehai Wu, and Hongwei Zhu. Wearable and Highly Sensitive Graphene Strain Sensors for Human Motion Monitoring. *Advanced Functional Materials*, 24(29):4666–4670, 2014.

[9] A. H. Castro Neto, F. Guinea, N. M. R. Peres, K. S. Novoselov, and A. K. Geim. The electronic properties of graphene. *Reviews of Modern Physics*, 81(1):109–162, 2009.

[10] Jingwei Bai and Yu Huang. Fabrication and electrical properties of graphene nanoribbons. *Materials Science and Engineering: R: Reports*, 70(3-6):341–353, 2010.

[11] Xiaochen Dong, Ching-Yuan Su, Wenjing Zhang, Jianwen Zhao, Qidan Ling, Wei Huang, Peng Chen, and Lain-Jong Li. Ultra-large single-layer graphene obtained from solution chemical reduction and its electrical properties. *Physical Chemistry Chemical Physics*, 12(9):2164, 2010.

[12] Changgu Lee, Xiaoding Wei, Jeffrey W Kysar, and James Hone. Measurement of the elastic properties and intrinsic strength of monolayer graphene. *Science*, 321(5887):385–8, 2008.

[13] Alexander A Balandin, Suchismita Ghosh, Wenzhong Bao, Irene Calizo, Desalegne Teweldebrhan, Feng Miao, and Chun Ning Lau. Superior Thermal Conductivity of Single-Layer Graphene. *Nano Letters*, 8(3):902–907, 2008.

[14] André K. Geim and K. S. Novoselov. The rise of graphene. *Nature Materials*, 6(3):183–191, 2007.

[15] Gunho Jo, Minhyeok Choe, Sangchul Lee, Woojin Park, Yung Ho Kahng, and Takhee Lee. The application of graphene as electrodes in electrical and optical devices. *Nanotechnology*, 23(11):112001, 2012.

[16] André K. Geim. Graphene: Status and Prospects. *Science*, 324(5934):1530–1534, 2009.

[17] Steven Cranford, Dipanjan Sen, and Markus J. Buehler. Meso-origami: Folding multilayer graphene sheets. *Applied Physics Letters*, 95(12):123121, 2009.

[18] Zhiping Xu and Markus J Buehler. Geometry Controls Conformation of Graphene Sheets: Membranes, Ribbons, and Scrolls. *ACS Nano*, 4(7):3869–3876, 2010.

[19] Jianfeng Zang, Seunghwa Ryu, Nicola Pugno, Qiming Wang, Qing Tu, Markus J. Buehler, and Xuanhe Zhao. Multifunctionality and control of the crumpling and unfolding of large-area graphene. *Nature Materials*, 12(4):321–325, 2013.

[20] Steven W. Cranford and Markus J. Buehler. Packing efficiency and accessible surface area of crumpled graphene. *Physical Review B*, 84(20):205451, 2011.

[21] Jianfeng Zang, Changyong Cao, Yaying Feng, Jie Liu, and Xuanhe Zhao. Stretchable and High-Performance Supercapacitors with Crumpled Graphene Papers. *Scientific Reports*, 4:6492, 2014.

[22] F. H. L. Koppens, T. Mueller, Ph. Avouris, A. C. Ferrari, M. S. Vitiello, and M. Polini. Photodetectors based on graphene, other two-dimensional materials and hybrid systems. *Nature Nanotechnology*, 9(10):780–793, 2014.

[23] Guanghong Zeng, Yibo Xing, Jian Gao, Zhiqiang Wang, and Xi Zhang. Unconventional Layer-by-Layer Assembly of Graphene Multilayer Films for Enzyme-Based Glucose and Maltose Biosensing. *Langmuir*, 26(18):15022–15026, 2010.

[24] K S Novoselov, A K Geim, S V Morozov, D Jiang, Y Zhang, S V Dubonos, I V Grigorieva, and A A Firsov. Electric field effect in atomically thin carbon films. *Science*, 306(5696):666–9, 2004.

[25] L A Falkovsky. Optical properties of graphene. *Journal of Physics: Conference Series*, 129(1):012004, 2008.

[26] F. Bonaccorso, Z. Sun, T. Hasan, and A. C. Ferrari. Graphene photonics and optoelectronics. *Nature Photonics*, 4(9):611–622, 2010.

[27] Changyong Cao, Yaying Feng, Jianfeng Zang, Gabriel P. López, and Xuanhe Zhao. Tunable lotus-leaf and rose-petal effects via graphene paper origami. *Extreme Mechanics Letters*, 4:18–25, 2015.

[28] Charalampos Androulidakis, Emmanuel N. Koukaras, John Parthenios, George Kalosakas, Konstantinos Papagelis, and Costas Galiotis. Graphene flakes under controlled biaxial deformation. *Scientific Reports*, 5:18219, 2015.

[29] Zheling Li, Ian A. Kinloch, Robert J. Young, Kostya S. Novoselov, George Anagnostopoulos, John Parthenios, Costas Galiotis, Konstantinos Papagelis, Ching-Yu Lu, and Liam Britnell. Deformation of Wrinkled Graphene. *ACS Nano*, 9(4):3917–3925, 2015.

[30] Xiang-Ying Ji, Yan-Ping Cao, and Xi-Qiao Feng. Micromechanics prediction of the effective elastic moduli of graphene sheet-reinforced polymer nanocomposites. *Modelling and Simulation in Materials Science and Engineering*, 18(4):045005, 2010.

[31] Shikai Deng and Vikas Berry. Wrinkled, rippled and crumpled graphene: an overview of formation mechanism, electronic properties, and applications. *Materials Today*, 19(4):197–212, 2016.

[32] Po-Yen Chen, Jaskiranjeet Sodhi, Yang Qiu, Thomas M Valentin, Ruben Spitz Steinberg, Zhongying Wang, Robert H Hurt, and Ian Y Wong. Multiscale Graphene Topographies Programmed by Sequential Mechanical Deformation. *Advanced Materials*, 28(18):3564–3571, 2016.

[33] Wei Yan, Wen-Yu He, Zhao-Dong Chu, Mengxi Liu, Lan Meng, Rui-Fen Dou, Yanfeng Zhang, Zhongfan Liu, Jia-Cai Nie, and Lin He. Strain and curvature induced evolution of electronic band structures in twisted graphene bilayer. *Nature communications*, 4:2159, 2013.

[34] Zhen Hua Ni, Ting Yu, Yun Hao Lu, Ying Ying Wang, Yuan Ping Feng, and Ze Xiang Shen. Uniaxial Strain on Graphene: Raman Spectroscopy Study and Band-Gap Opening. *ACS Nano*, 2(11):2301–2305, 2008.

[35] Chen Si, Zhimei Sun, and Feng Liu. Strain engineering of graphene: a review. *Nanoscale*, 8(6):3207–3217, 2016.

[36] Michael Cai Wang, SungGyu Chun, Ryan Steven Han, Ali Ashraf, Pilgyu Kang, and SungWoo Nam. Heterogeneous, Three-Dimensional Texturing of Graphene. *Nano Letters*, 15(3):1829–1835, 2015.

[37] Atsushi Takei, Lihua Jin, John W Hutchinson, and Hiroyuki Fujita. Ridge Localizations and Networks in Thin Films Compressed by the Incremental Release of a Large Equi-biaxial Pre-stretch in the Substrate. *Advanced Materials*, 26(24):4061–4067, 2014.

[38] Dominic Vella, José Bico, Arezki Boudaoud, Benoit Roman, and Pedro M Reis. The macroscopic delamination of thin films from elastic substrates. *Proceedings of the National Academy of Sciences of the United States of America*, 106(27):10901–6, 2009.

[39] Huanyu Cheng, Yihui Zhang, Keh-Chih Hwang, John A. Rogers, and Yonggang Huang. Buckling of a stiff thin film on a pre-strained bi-layer substrate. *International Journal of Solids and Structures*, 51(18):3113–3118, 2014.

[40] Z.Y. Huang, W. Hong, and Z. Suo. Nonlinear analyses of wrinkles in a film bonded to a compliant substrate. *Journal of the Mechanics and Physics of Solids*, 53(9):2101–2118, 2005.

[41] Bo Li, Yan-Ping Cao, Xi-Qiao Feng, and Huajian Gao. Mechanics of morphological instabilities and surface wrinkling in soft materials: a review. *Soft Matter*, 8(21):5728, 2012.

[42] Haixia Mei, Rui Huang, Jun Young Chung, Christopher M. Stafford, and Hong-Hui Yu. Buckling modes of elastic thin films on elastic substrates. *Applied Physics Letters*, 90(15):151902, 2007.

[43] Lihua Jin, Atsushi Takei, and John W. Hutchinson. Mechanics of wrinkle/ridge transitions in thin film/substrate systems. *Journal of the Mechanics and Physics of Solids*, 81:22–40, 2015.

[44] Xiu Yang, Yan Zhao, Jixun Xie, Xue Han, Juanjuan Wang, Chuanyong Zong, Haipeng Ji, Jingxin Zhao, Shichun Jiang, Yanping Cao, and Conghua Lu. Bioinspired Fabrication of Free-Standing Conducting Films with Hierarchical Surface Wrinkling Patterns. *ACS nano*, 10(3):3801–8, 2016.

[45] Wubo Wan, Zongbin Zhao, Han Hu, Xiaojuan Hao, Timothy C. Hughes, He Ma, Lujun Pan, and Jieshan Qiu. Folding of graphene into elastic nanobelts. *Carbon*, 76:46–53, 2014.

[46] Teng Zhang, Xiaoyan Li, and Huajian Gao. Defects controlled wrinkling and topological design in graphene. *Journal of the Mechanics and Physics of Solids*, 67:2–13, 2014.

[47] Marin Petrović, Jerzy T. Sadowski, Antonio Šiber, and Marko Kralj. Wrinkles of graphene on Ir(111): Macroscopic network ordering and internal multi-lobed structure. *Carbon*, 94:856–863, 2015.

[48] Emmanuel N. Koukaras, Charalampos Androulidakis, George Anagnostopoulos, Konstantinos Papagelis, and Costas Galiotis. Compression behavior of simply-supported and fully embedded monolayer graphene: Theory and experiment. *Extreme Mechanics Letters*, 2016.

[49] J. Henry Hinnefeld, Stephen T. Gill, Shuze Zhu, William J. Swanson, Teng Li, and Nadya Mason. Reversible Mechanical and Electrical Properties of Ripped Graphene. *Physical Review Applied*, 3(1):014010, 2015.

[50] Pilgyu Kang, Michael Cai Wang, Peter M Knapp, and SungWoo Nam. Crumpled Graphene Photodetector with Enhanced, Strain-Tunable, and Wavelength-Selective Photoresponsivity. *Advanced Materials*, 28(23):4639–4645, 2016.

[51] A.G. Pandolfo and A.F. Hollenkamp. Carbon properties and their role in supercapacitors. *Journal of Power Sources*, 157(1):11–27, 2006.

[52] Changyong Cao, Hon Fai Chan, Jianfeng Zang, Kam W Leong, and Xuanhe Zhao. Harnessing Localized Ridges for High-Aspect-Ratio Hierarchical Patterns with Dynamic Tunability and Multifunctionality. *Advanced Materials*, 26(11):1763–1770, 2014.

[53] Julia A. Baimova, Leysan Kh. Rysaeva, Bo Liu, Sergey V. Dmitriev, and Kun Zhou. From flat graphene to bulk carbon nanostructures. *physica status solidi (b)*, 252(7):1502–1507, 2015.

[54] Waleed M. A. El Rouby. Crumpled graphene: preparation and applications. *RSC Adv.*, 5(82):66767–66796, 2015.

[55] Jian-Nan Wang, Yong-Lai Zhang, Yan Liu, Wanhua Zheng, Luke P Lee, and Hong-Bo Sun. Recent developments in superhydrophobic graphene and graphene-related materials: from preparation to potential applications. *Nanoscale*, 7(16):7101–7114, 2015.

[56] Qiming Wang and Xuanhe Zhao. Beyond wrinkles: Multimodal surface instabilities for multifunctional patterning. *MRS Bulletin*, 41(02):115–122, 2016.

[57] Zhao Zhang and Teng Li. Graphene morphology regulated by nanowires patterned in parallel on a substrate surface. *Journal of Applied Physics*, 107(10):103519, 2010.

[58] Zhao Zhang and Teng Li. Determining graphene adhesion via substrate-regulated morphology of graphene. *Journal of Applied Physics*, 110(8):083526, 2011.

[59] Teng Li and Zhao Zhang. Substrate-regulated morphology of graphene. *Journal of Physics D: Applied Physics*, 43(7):075303, 2010.

[60] Zachary H. Aitken and Rui Huang. Effects of mismatch strain and substrate surface corrugation on morphology of supported monolayer graphene. *Journal of Applied Physics*, 107(12):123531, 2010.

[61] Cengiz S. Ozkan, Markus J. Buehler, Nicola Maria Pugno, and Kang Wang. Introduction. *Journal of Materials Research*, 28(07):909–911, 2013.

[62] Rubén Mas-Ballesté, Cristina Gómez-Navarro, Julio Gómez-Herrero, and Félix Zamora. 2D materials: to graphene and beyond. *Nanoscale*, 3(1):20–30, 2011.

[63] Akihiro Kushima, Xiaofeng Qian, Peng Zhao, Sulin Zhang, and Ju Li. Ripplocations in van der Waals Layers. *Nano Letters*, 15(2):1302–1308, 2015.

[64] André K. Geim and I. V. Grigorieva. Van der Waals heterostructures. *Nature*, 499(7459):419–425, 2013.

[65] Lin Feng, Yanan Zhang, Jinming Xi, Ying Zhu, Nü Wang, Fan Xia, and Lei Jiang. Petal Effect: A Superhydrophobic State with High Adhesive Force. *Langmuir*, 24(8):4114–4119, 2008.

[66] Lin Feng, S. Li, Y. Li, Huanjun Li, Lingjuan Zhang, Jin Zhai, Yanlin Song, Biqian Liu, Lei Jiang, and Daoben Zhu. Super-Hydrophobic Surfaces: From Natural to Artificial. *Advanced Materials*, 14(24):1857–1860, 2002.

[67] Edson P. Bellido and Jorge M. Seminario. Molecular Dynamics Simulations of Folding of Supported Graphene. *The Journal of Physical Chemistry C*, 114(51):22472–22477, 2010.

[68] R. Ansari, S. Ajori, and B. Motevalli. Mechanical properties of defective single-layered graphene sheets via molecular dynamics simulation. *Superlattices and Microstructures*, 51(2):274–289, 2012.

[69] Chao Tang, Lijun Meng, Lizhong Sun, Kaiwang Zhang, and Jianxin Zhong. Molecular dynamics study of ripples in graphene nanoribbons on 6H-SiC(0001): Temperature and size effects. *Journal of Applied Physics*, 104(11):113536, 2008.

[70] Lijuan Meng, Qing Sun, Jinlan Wang, and Feng Ding. Molecular Dynamics Simulation of Chemical Vapor Deposition Graphene Growth on Ni (111) Surface. *The Journal of Physical Chemistry C*, 116(10):6097–6102, 2012.

[71] C. Y. Wang, K. Mylvaganam, and L. C. Zhang. Wrinkling of monolayer graphene: A study by molecular dynamics and continuum plate theory. *Physical Review B*, 80(15):155445, 2009.

[72] Maxim V. Fedorov and R. M. Lynden-Bell. Probing the neutral graphene-ionic liquid interface: insights from molecular dynamics simulations. *Physical Chemistry Chemical Physics*, 14(8):2552, 2012.

[73] S. P. Xiao and T. Belytschko. A bridging domain method for coupling continua with molecular dynamics. *Computer Methods in Applied Mechanics and Engineering*, 193(17-20):1645–1669, 2004.

[74] Gun Do Lee, C. Z. Wang, Euijoon Yoon, Nong Moon Hwang, and K. M. Ho. Vacancy defects and the formation of local haeckelite structures in graphene from tight-binding molecular dynamics. *Physical Review B - Condensed Matter and Materials Physics*, 74(24):245411, 2006.

[75] Wu Qin, Xin Li, Wen-Wen Bian, Xiu-Juan Fan, and Jing-Yao Qi. Density functional theory calculations and molecular dynamics simulations of the adsorption of biomolecules on graphene surfaces. *Biomaterials*, 31(5):1007–1016, 2009.

[76] Zhonghua Ni, Hao Bu, Min Zou, Hong Yi, Kedong Bi, and Yunfei Chen. Anisotropic mechanical properties of graphene sheets from molecular dynamics. *Physica B: Condensed Matter*, 405(5):1301–1306, 2010.

[77] Q.X. X. Pei, Y.W. W. Zhang, and V.B. B. Shenoy. A molecular dynamics study of the mechanical properties of hydrogen functionalized graphene. *Carbon*, 48(3):898–904, 2010.

[78] Jiuning Hu, Xiulin Ruan, and Yong P. Chen. Thermal conductivity and thermal rectification in graphene nanoribbons: a molecular dynamics study. *Nano Letters*, 9(7):2730–2735, 2009.

[79] Mark E. Tuckerman. *Statistical Mechanics: Theory and Molecular Simulation*. Oxford University Press, 2010.

[80] Roger Bowley and Sánchez Mariana. *Introductory Statistical Mechanics*. Oxford University Press, 1996.

[81] Stephen C. Harvey, Robert K.-Z. Tan, and Thomas E. Cheatham. The flying ice cube: Velocity rescaling in molecular dynamics leads to violation of energy equipartition. *Journal of Computational Chemistry*, 19(7):726–740, 1998.

[82] Hideo Kaburaki, Ju Li, and Sidney Yip. Thermal Conductivity of Solid Argon by Classical Molecular Dynamics. *MRS Proceedings*, 538:503, 1998.

[83] Boris D Lubachevsky. How to simulate billiards and similar systems. *Journal of Computational Physics*, 94(2):255–283, 1991.

[84] Steve Plimpton. Fast Parallel Algorithms for Short-Range Molecular Dynamics. *Journal of Computational Physics*, 117(1):1–19, 1995.

[85] Philip M. Morse. Diatomic Molecules According to the Wave Mechanics. II. Vibrational Levels. *Physical Review*, 34(1):57–64, 1929.

[86] Steven J. Stuart, Alan B. Tutein, and Judith A. Harrison. A reactive potential for hydrocarbons with intermolecular interactions. *The Journal of Chemical Physics*, 112(14):6472, 2000.

[87] Donald W. Brenner. Empirical potential for hydrocarbons for use in simulating the chemical vapor deposition of diamond films. *Physical Review B*, 42(15):9458–9471, 1990.

[88] Donald W Brenner, Olga A Shenderova, Judith A Harrison, Steven J Stuart, Boris Ni, and Susan B Sinnott. A second-generation reactive empirical bond order (REBO) potential energy expression for hydrocarbons. *Journal of Physics: Condensed Matter*, 14(4):783–802, 2002.

[89] Emmanuel N. Koukaras, George Kalosakas, Costas Galiotis, and Konstantinos Papagelis. Phonon properties of graphene derived from molecular dynamics simulations. *Scientific Reports*, 5:12923, 2015.

[90] Vivek B. Shenoy, Chilla Damodara Reddy, and Yong-Wei Zhang. Spontaneous Curling of Graphene Sheets with Reconstructed Edges. *ACS Nano*, 4(8):4840–4844, 2010.

[91] V. B. Shenoy, C. D. Reddy, A. Ramasubramaniam, and Y. W. Zhang. Edge-Stress-Induced Warping of Graphene Sheets and Nanoribbons. *Physical Review Letters*, 101(24):245501, 2008.

[92] H. Zhao, K. Min, and N. R. Aluru. Size and Chirality Dependent Elastic Properties of Graphene Nanoribbons under Uniaxial Tension. *Nano Letters*, 9(8):3012–3015, 2009.

[93] J. IIja Siepmann, Sami Karaborni, and Berend Smit. Simulating the critical behaviour of complex fluids. *Nature*, 365(6444):330–332, 1993.

[94] A.I. Kitaygorodsky. The interaction curve of non-bonded carbon and hydrogen atoms and its application. *Tetrahedron*, 14(3-4):230–236, 1961.

[95] Muse Degefe and Avinash Parashar. Effect of non-bonded interactions on failure morphology of a defective graphene sheet. *Materials Research Express*, 3(4):045009, 2016.

[96] Luis Ruiz, Wenjie Xia, Zhaoxu Meng, and Sinan Keten. A coarse-grained model for the mechanical behavior of multi-layer graphene. *Carbon*, 82:103–115, 2015.

[97] Thomas C. O'Connor, Jan Andzelm, Mark O. Robbins, Thomas C O'Connor, Jan Andzelm, and Mark O. Robbins. AIREBO-M: a reactive model for hydrocarbons at extreme pressures. *The Journal of chemical physics*, 142(2):024903, 2015.

[98] Talal Al-Mulla, Zhao Qin, and Markus J Buehler. Crumpling deformation regimes of monolayer graphene on substrate: a molecular mechanics study. *Journal of Physics: Condensed Matter*, 27(34):345401, 2015.

[99] Georgia Tsoukleri, John Parthenios, Konstantinos Papagelis, Rashid Jalil, Andrea C. Ferrari, Andre K. Geim, Kostya S. Novoselov, and Costas Galiotis. Subjecting a Graphene Monolayer to Tension and Compression. *Small*, 5(21):2397–2402, 2009.

[100] Yu Zhang and Feng Liu. Maximum asymmetry in strain induced mechanical instability of graphene: Compression versus tension. *Applied Physics Letters*, 99(24):241908, 2011.

[101] Teng Li and Zhao Zhang. Snap-Through Instability of Graphene on Substrates. *Nanoscale Research Letters*, 5(1):169–173, 2010.

[102] F. Guinea, M. I. Katsnelson, and A. K. Geim. Energy gaps and a zero-field quantum Hall effect in graphene by strain engineering. *Nature Physics*, 6(1):30–33, 2010.

[103] Da Zhan, Jiaxu Yan, Linfei Lai, Zhenhua Ni, Lei Liu, and Zexiang Shen. Engineering the Electronic Structure of Graphene. *Advanced Materials*, 24(30):4055–4069, 2012.

[104] Vitor M. Pereira and A. H. Castro Neto. Strain Engineering of Graphene's Electronic Structure. *Physical Review Letters*, 103(4):046801, 2009.

[105] Zhao Qin, Michael Taylor, Mary Hwang, Katia Bertoldi, and Markus J. Buehler. Effect of Wrinkles on the Surface Area of Graphene: Toward the Design of Nanoelectronics. *Nano Letters*, 14(11):6520–6525, 2014.

[106] Jian Zou, Baohua Ji, Xi-Qiao Feng, and Huajian Gao. Self-Assembly of Single-Walled Carbon Nanotubes into Multiwalled Carbon Nanotubes in Water: Molecular Dynamics Simulations. *Nano Letters*, 6(3):430–434, 2006.

[107] Farid F. Abraham and Y. Singh. The structure of a hard-sphere fluid in contact with a soft repulsive wall. *The Journal of Chemical Physics*, 67(5):2384, 1977.

[108] Chun Hung Lui, Li Liu, Kin Fai Mak, George W Flynn, and Tony F Heinz. Ultraflat graphene. *Nature*, 462(7271):339–341, 2009.

[109] William Humphrey, Andrew Dalke, and Klaus Schulten. VMD: Visual molecular dynamics. *Journal of Molecular Graphics*, 14(1):33–38, 1996.

[110] Ju Li. AtomEye: an efficient atomistic configuration viewer. *Modelling and Simulation in Materials Science and Engineering*, 11(2):173–177, 2003.

[111] Steven P Koenig, Narasimha G Boddeti, Martin L Dunn, and J Scott Bunch. Ultrastrong adhesion of graphene membranes. *Nature Nanotechnology*, 6(9):543–546, 2011.

[112] Yufeng Guo and Wanlin Guo. Structural transformation of partially confined copper nanowires inside defected carbon nanotubes. *Nanotechnology*, 17(18):4726–4730, 2006.

[113] Byron D Gates, Qiaobing Xu, Michael Stewart, Declan Ryan, C Grant Willson, and George M Whitesides. New Approaches to Nanofabrication: Molding, Printing, and Other Techniques. *Chemical Reviews*, 105(4):1171–1196, 2005.

[114] Dipanjan Sen, Kostya S Novoselov, Pedro M Reis, and Markus J Buehler. Tearing graphene sheets from adhesive substrates produces tapered nanoribbons. *Small*, 6(10):1108–16, 2010.

[115] Ted L. Anderson and T. L. Anderson. *Fracture Mechanics: Fundamentals and Applications, Third Edition.* CRC Press, 2005.

[116] S. Ho and Z. Suo. Tunneling Cracks in Constrained Layers. *Journal of Applied Mechanics*, 60(4):890, 1993.

[117] Markus J. Buehler and Sinan Keten. Colloquium : Failure of molecules, bones, and the Earth itself. *Reviews of Modern Physics*, 82(2):1459–1487, 2010.

[118] S. Azari, M. Papini, and J. K. Spelt. Effect of Surface Roughness on the Performance of Adhesive Joints Under Static and Cyclic Loading. *The Journal of Adhesion*, 86(7):742–764, 2010.

[119] K. Zhang and M. Arroyo. Adhesion and friction control localized folding in supported graphene. *Journal of Applied Physics*, 113(19):193501, 2013.